https://doi.org/10.5194/egusphere-2025-6563
Preprint. Discussion started: 13 January 2026

Buoyancy and polarity driven accumulation of dissolved organic matter in the sea surface microlayer during a phytoplankton bloom

Jasper Zöbelein[1], Shubham Sawle[2], Gernot Friedrichs[2,3], Mariana Ribas-Ribas[1], Carola Lehners[1], Katharina Paetz[1], Maximilian Pflaum[2], Hannelore Waska[1]

[1]Institute for Chemistry and Biology of the Marine Environment (ICBM), School of Mathematics and Science, Carl von Ossietzky Universität Oldenburg, Oldenburg, Germany
[2]Institute of Physical Chemistry, Christian-Albrechts-University Kiel, Kiel, Germany
[3]KMS Kiel Marine Science-Centre for Interdisciplinary Marine Science, Kiel University, Kiel, Germany

Correspondence to: Jasper Zöbelein (jasper.zoebelein@uni-oldenburg.de)

Abstract

The sea surface microlayer (SML) is only 1-1000 µm thick but resembles a biologically and geochemically very active boundary that modulates the exchange of energy and matter between the ocean and atmosphere. Globally, the SML accumulates up to 200 Tg C yr^{-1} of organic matter, comparable to sedimentation rates on the oceans' seafloor. Yet, the mechanisms governing the accumulation and transformation of dissolved organic matter (DOM) in the SML remain poorly understood. Exposed to rapid changes of physical, biological, and photochemical conditions, the organic matter pool in the SML often shows heterogeneous distribution patterns, and a clear differentiation between SML and underlying water (ULW) is not always captured during *in situ* observations. In our mesocosm study, we initiated a phytoplankton bloom under controlled conditions, excluding physical influences like currents, waves, and precipitation. We tested three major hypotheses for DOM enrichment and compartmentalisation in the SML: enhanced *in situ* biogenic production and processing; physicochemical sorting by polarity and buoyancy; and selective degradation. Our results revealed that buoyancy-driven enrichment of DOM in the SML, fueled by local phytoplankton exudates and their subsequent breakdown, is key to DOM accumulation in the SML-during and after phytoplankton blooms. Untargeted ultra-high-resolution mass spectrometry, complemented by functional group analysis via Fourier transform infrared spectroscopy, showed that particulary carbohydrate compounds became highly enriched in the SML. We also found evidence for accumulation of hydrophobic DOM of biogenic origin, such as lipid- and protein-like compounds, but the related polarity-driven compartmentalisation played a minor role. Moreover, no selective bio- and photodegradation patterns in the SML compared to the ULW took place. We conclude that under exclusively biogenic conditions, sugars and sugar-related compounds are the main drivers of SML compartmentalisation, and we suggest that phytoplankton-induced "carbo-slicks" could be the pioneer stage of a succession of SML organic geochemistry in natural environments.

https://doi.org/10.5194/egusphere-2025-6563
Preprint. Discussion started: 13 January 2026

1 Introduction

The sea surface microlayer (SML) is a dynamic and complex interface connecting the ocean and the atmosphere (Liss and Duce, 1997; Cunliffe et al., 2013; Wurl et al., 2017). Although it is only 1-1000 µm thick, it is, functioning as a unique biogeochemical reactor that mediates air-sea gas and energy exchanges, thereby playing a crucial role in global biogeochemical processes (Cunliffe and Murrell, 2009). The SML is a highly dynamic system, strongly influenced by wind and waves (Cunliffe and Murrell, 2009). The residence time of organic matter within the SML is likely very short, ranging from seconds to days (Carlson, 1993; Cunliffe et al., 2013; Wurl et al., 2017). Independent from this timescale, the SML can quickly re-establish itself after wave disruption (Wurl et al., 2011). Under low-wind conditions, a SML with accumulated organic matter (OM) can appear as visible slick patches because capillary waves (wavelength < 2 cm) are dampened, reducing energy transfer and altering the light-reflecting properties of the ocean surface (Hunter and Liss, 1981). Its dynamic nature presents substantial challenges for sampling, particularly when large volumes of SML must be collected over short time scales (Cunliffe and Wurl, 2014). These constraints complicate efforts to comprehensively characterise the SML's dynamic formation, degradation, and its impact on the global carbon cycle. However, recent advances in analytical techniques and interdisciplinary research over recent decades have brought renewed attention to the SML, enabling a deeper understanding of its ecological and biogeochemical significance (Engel et al., 2017; Ribas-Ribas et al., 2017; Wurl et al., 2024).

Estimates suggest that up to 200 Tg C yr^{-1} accumulate in the SML, a quantity comparable to organic carbon (OC) sedimentation rates to the ocean's seabed (Ellison et al., 1999). Several hypotheses have been proposed to explain the accumulation of photosynthetically produced organic matter (OM) in the SML, which can broadly be classed into two major driving forces: (1) compartmentalisation related to physical aggregation through adsorption on rising bubbles and buoyant particles, or turbulent mixing (Liss and Duce, 1997; Passow, 2002; Engel et al., 2004; Wurl and Holmes, 2008); (2) compartmentalisation resulting from the intrinsic chemical properties of particulate and dissolved organic matter (POM and DOM), such as polarity, aromaticity, and functional groups with lipophilic or amphiphilic properties (Marty and Saliot, 1976; Carlson and Mayer, 1980; Carlson, 1982; Lechtenfeld et al., 2013).

Despite its location and surface-active properties, the SML is not exclusively composed of simple surface-active agents such as fatty acids or other strong surfactants, nor is it dominated by anthropogenic pollutants like oils, except in some coastal regions (Blaženka Gašparović et al., 1998a; Wurl and Obbard, 2004; Cunliffe and Murrell, 2009). Although surfactants are particularly enriched in the SML (Silva et al., 2025), it is hypothesised that OM in the SML is a polydisperse mixture, originates from a variety of diagenetic processes, and mainly comprises phytoplankton exudates and their degradation products (Žutić et al., 1981; Blaženka Gašparović et al., 1998b; Wurl et al., 2009; Barthelmeß and Engel, 2022). The surfactants themselves may consist of complex polymeric materials rich in hydroxyl, carboxyl, and protein-like components (Passow et al., 1994; B. Gašparović et al., 1998; Croot et al., 2007; Thornton, 2014). Overall, the composition OM within the SML is heavily influenced by the diversity of phytoplankton present but generally entails lipids, proteins, and carbohydrates (Myklestad, 1995; Penna,

https://doi.org/10.5194/egusphere-2025-6563
Preprint. Discussion started: 13 January 2026

1999; Croot et al., 2007; Wurl and Holmes, 2008). Conventionally, only a fraction of these biopolymers can be determined using component-specific targeted methods, comprising <10% of the SML-OM (Minor et al., 2014; Petras et al., 2017; Zark et al., 2017; Bergmann et al., 2024). To this day, the exact chemical structures of most of the countless of compounds remain unknown. The dissolved organic matter (DOM) pool that results from abiotic and biological turnover of photosynthetic products is therefore referred to as the "DOM geometabolome", a chemically diverse mixture of compounds that cannot be resolved by analytical methods targeting known biomolecules (Niggemann et al., 2011; Zark et al., 2017).

Based on the DOM geometabolome concept, the value of a non-targeted and holistic analytical approach becomes apparent. Analytical methods such as ultra-high resolution Fourier-transform ion-cyclotron-resonance mass-spectrometry (FT-ICR-MS) enable a simultaneous assessment of molecular signatures associated with multiple enrichment processes. For this analysis, DOM from water samples must be free of salt and pre-concentrated, which can be achieved through solid-phase extraction (Dittmar et al., 2008). FT-ICR-MS has become a state-of-the-art analytical tool for examining highly complex DOM mixtures (Koch et al., 2008), since its high mass accuracy and resolution enable the identification of several thousand molecular formulas per sample. Previous FT-ICR-MS studies on estuarine DOM in the SML found that structural indicators of polarity, like elemental H/C and O/C ratios and aromaticity indices, differed between SML and underlying water (ULW), pointing to an enrichment of less polar compounds i the SML. Furthermore, they revealed a high molecular variability of SML surfactants (Schmitt-Kopplin et al., 2012; Lechtenfeld et al., 2013; Coffey et al., 2025a). However, FT-ICR-MS studies focusing on SML-DOM remain sparse, and the technique has faced criticism because it does not fully reveal chemical structures and may underestimate the presence of known polar biomolecules like carbohydrates (Raeke et al., 2016). Complementary to FT-ICR-MS, Fourier-transform infrared (FTIR) spectroscopy is widely used to characterise DOM on a structural level (e.g. Abdulla et al., 2010; Minor et al., 2014; Soong et al., 2014; Duan et al., 2024). FTIR spectroscopy probes vibrations of chemical bonds, resulting in a spectrum whose band positions and shapes reflect functional groups and their local environments (Griffiths and Haseth, 2007). Because absorbance in FTIR follows the Beer–Lambert law, it can be used to obtain quantitative (or semi-quantitative) information on functional groups, such as aromatic, aliphatic, carboxyl, hydroxyl, amide, and polysaccharide moieties. Although it has lower resolution, FTIR can be used to extract targeted band-integral changes to complement FT-ICR-MS molecular formula data, thereby linking compositional changes to specific functional transformations in DOM.

Through a combination of FT-ICR-MS and FTIR, this study aimed at investigating the bio- and geochemical evolution of early diagenetic DOM in the SML during a mesocosm phytoplankton bloom, tracking its temporal changes in the SML and ULW. To bypass the challenges of SML investigations under physical impacts caused by wind, waves, currents and rain, the joint research unit 'Biogeochemical Processes and Air-Sea Exchange in the Sea-Surface Microlayer' (BASS) conducted a mesocosm study under strictly controlled conditions, focusing mainly on biogenic influences (Bibi et al., 2025). By inducing a phytoplankton bloom through nutrient addition to pretreated natural seawater containing microbial autotrophic and heterotrophic communities from the nearby Jade Bay, we were able to trace an *in situ*-produced SML slick in isolation and

https://doi.org/10.5194/egusphere-2025-6563
Preprint. Discussion started: 13 January 2026

study its genesis and subsequent decay. Throughout this study, we expected (1) an accumulation of photosynthetically produced carbohydrate-rich DOM in the SML compared to the ULW. Additionally, we examined (2) the role of molecular polarity i.e. whether amphiphilic and lipophilic substances accumulated in the SML during this bloom event. Finally, we anticipated (3) increased photodegradation and biodegradation of the SML-DOM composition relative to the ULW.

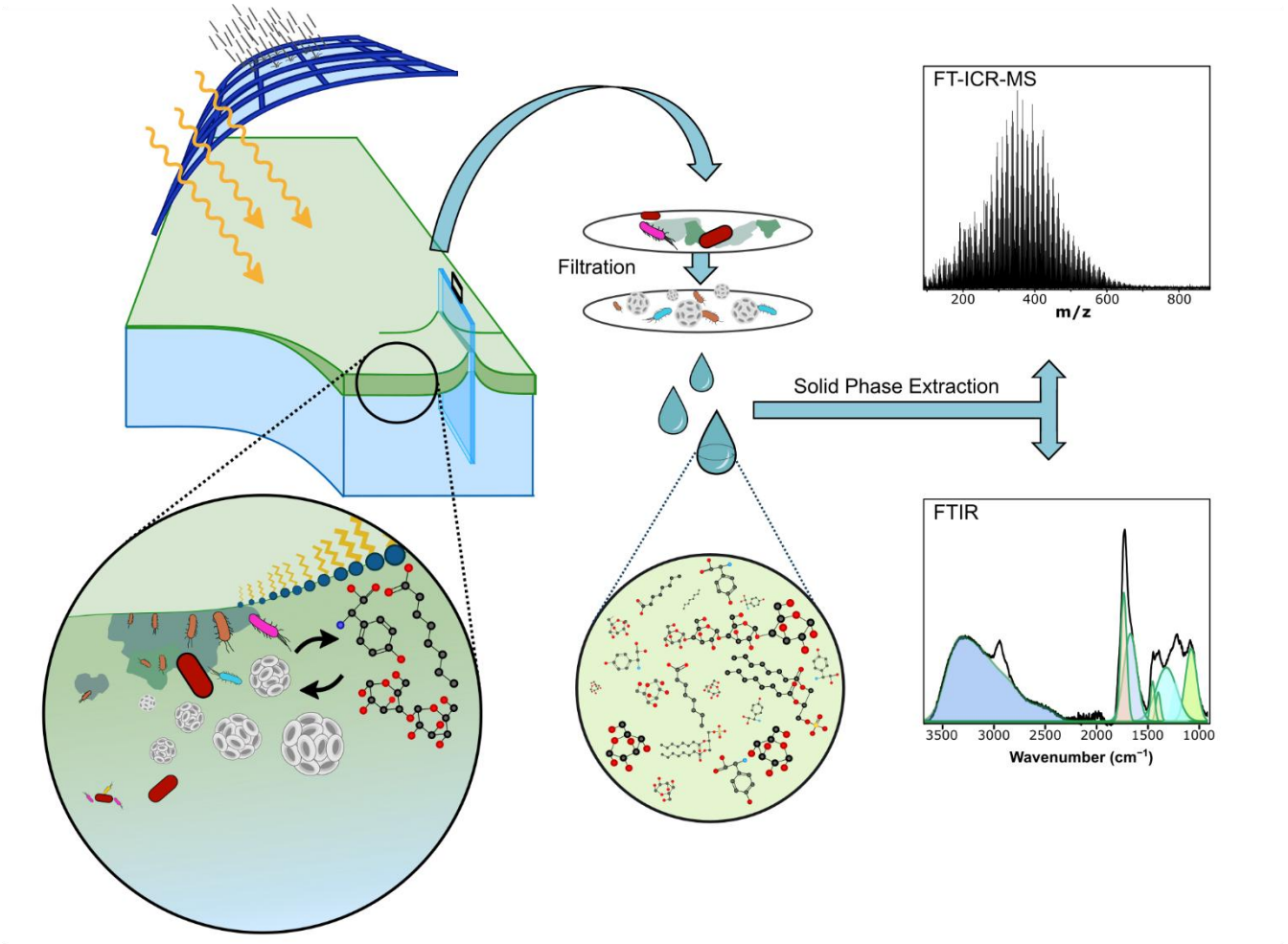

Fig. 1: Schematic overview of the mesocosm setup at the sea surface facility (SURF) in Wilhelmshaven during this investigation, and the sample processing workflow for DOM compositional analysis.

2 Methods

2.1 Mesocosm setup & sampling strategy

A mesocosm study was conducted for 33 days between May 15 and June 16, 2023, to investigate the genesis of a SML during an induced phytoplankton bloom (Fig. 1). The mesocosm was set up at the Sea Surface Facility (SURF), at the Centre for

https://doi.org/10.5194/egusphere-2025-6563
Preprint. Discussion started: 13 January 2026

Marine Sensor Technology (ZfMArS), Institute of Chemistry and Biology of the Marine Environment (ICBM, Wilhelmshaven, Germany). SURF is an outdoor mesocosm developed to simulate and study ocean processes at the air-sea interface under controlled conditions. With a basin measuring 8.5 m long, 2 m wide, and 1 m in depth, it has a capacity of up to 17,000 L of seawater. The basin can be covered by a light-transmissive, retractable roof that allows UV exposure from natural light while shielding from wind and rain, maintaining an uninterrupted surface.

SURF was filled with natural seawater from the nearby Jade Bay (53° 28' 42'' N, 8° 12' 15'' E) to replicate natural conditions. The late spring period was selected to ensure a low initial phytoplankton abundance in the utilised seawater. Additionally, the seawater was filtered, skimmed, and UV-treated at the start of the study to further reduce particle concentration and biological activity. To induce and sustain a phytoplankton bloom, inorganic nitrogen, phosphorus, and silicate were added on May 26, May 31, and June 01, 2023. During the mesocosm study, a Phyto-PAM fluorometer (Walz, Germany) was used to monitor *in situ* shifts in Chlorophyll *a* (Chl*a*) concentration. A more detailed description of the mesocosm setup and procedures is provided by Bibi et al. (2025).

SML samples were collected using the glass plate technique (Cunliffe and Wurl, 2014). A pre-rinsed glass plate (30 × 25 cm) was vertically immersed in the mesocosm seawater and moved slowly away from the point of entry (Fig. 1). The glass plate was pulled out of the water at a controlled speed of 5 - 6 cm s^{-1}. This allowed a thin (<1 mm), undisturbed SML film to adhere to the glass plate. The film was then removed using a squeegee and transferred through an acid-washed glass funnel into an acid-washed high-density polyethylene (HDPE) bottle. Consecutive dips were conducted at different locations within the mesocosm, and the collected samples were pooled to obtain an integrated representation of the SML. Alternating sampling times between the morning (one hour after sunrise) and the afternoon (10 hours after sunrise) enabled the collection of samples with different levels of sunlight exposure. To reduce sampling frequency and maintain the integrity of the SML, only about 30% was sampled daily. To minimise contamination, all handling of the glass plate was performed using ultrapure water (UPW)-rinsed nitrile gloves.

2.2 Dissolved organic carbon, total dissolved nitrogen, dissolved organic nitrogen & humic-like fluorescent dissolved organic carbon

Water samples for dissolved organic carbon (DOC), and humic-like fluorescent dissolved organic matter (FDOM) analysis were filtered with an acid-rinsed 50 mL polyethylene syringe through a polypropylene filter holder (Advantec, USA) containing combusted stacked glass fibre filters (450°C for 4 h, GMF, 2.0 µm and GF/F 0.7 µm pore sizes, 47 mm diameter, Whatman, UK). Additional water samples were filtered under vacuum through a reusable polysulfone bottle-top filter holder (Thermo Scientific Nalgene, US) containing polycarbonate filters (5.0 µm, 3.0 µm and finally 0.2 µm, 47 mm diameter, Nuclepore Track-Etch Membrane, Whatman, UK). All filtered samples were stored at natural pH in acid-rinsed HDPE bottles at −18 °C.

https://doi.org/10.5194/egusphere-2025-6563
Preprint. Discussion started: 13 January 2026

After thawing and sonication, 2 mL aliquots were transferred into combusted 20 mL glass vials and diluted to 10 mL with low-carbon ultrapure water acidified to pH 2 with HCl (25%, AnalaR NORMAPUR, VWR, USA). DOC concentrations were measured using Shimadzu TOC Analysers (TOC-L or TOC-VCPH) following the high-temperature catalytic oxidation method (Sugimura and Suzuki, 1988; Badr et al., 2003). DOC was detected as CO_2 with a non-dispersive infrared (IR) gas analyser. Each sample was injected four times; after removing outliers, the values were averaged. Accuracy and precision were verified using certified Atlantic deep-sea reference material (D.A. Hansell, University of Miami, FL, USA). A run was considered valid if the DOC concentration in the reference material remained between 41 and 44 µmol L^{-1} (µM), with accuracy and precision better than 5%. For calibration, 12 different concentrations of an L-arginine standard (Sigma, USA) were prepared and checked against a potassium hydrogen phthalate standard (Nacalai Tesque, Japan).

TDN values were obtained from GEOMAR, Kiel (Bibi et al. 2025). Duplicate samples were filtered through 0.45 µm GMF GD/X syringe filters (Whatman, UK) into 20 mL ampoules, which were pre-combusted (8 hours at 500°C). To acidify the samples, 20 µL of 30% HCl (Suprapure, Sigma-Aldrich, US) was added, after which they were immediately sealed and stored at +4°C until analysis. One duplicate was measured multiple times (n = 4), also using a high-temperature catalytic oxidation analyser coupled to a total dissolved nitrogen measurement unit (TOC-VCSH, Shimadzu). TDN was detected as NO_x via chemiluminescence. Sample-specific precision was calculated as the standard deviation of the four repeated measurements divided by the mean, showing a relative standard deviation (relSD) of 1.45 ±0.60% for TDN. The maximum relSD for technical replicates of TDN was 2.87%. For TDN calibration, four standard concentrations of potassium nitrate (Merck, Germany) were prepared.

Samples for inorganic nitrite (NO_2^-) and nitrate (NO_3^-) analysis were filtered with a cellulose acetate membrane filter (0.45 µm) (Bibi et al.). All nutrient samples were poisoned with mercury chloride and stored at 4 °C for further analysis. NO_2^- and NO_3^- concentrations were determined by the microtiter plate technique described by Schnetger and Lehners (2014). Dissolved organic nitrogen (DON) was calculated by subtracting the sum of inorganic nitrate (NO_x) from the TDN values (DON = TDN – NO_x).

For humic-like FDOM quantification, 4 mL aliquots of filtered water samples were measured directly after thawing and sonication, using a handheld fluorometer (AquaFluor 8000-010, Turner Instruments, USA). It has a sensitivity range of 0.03 - 1,000 ppb quinine sulphate equivalents and excites the sample at a wavelength of 375 nm while detecting emission at wavelengths >420 nm. These wavelengths are characteristic for terrestrial and aquatic humic-like organic matter (Waska et al., 2021). The values are expressed in relative fluorescence units (RFU).

2.3 Solid phase extraction of dissolved organic matter (SPE-DOM)

30 mL of filtered, thawed, sonicated, and acidified sample aliquots (pH = 2, HCl, 25%, AnalaR NORMAPUR, VWR, USA) were solid-phase extracted (SPE) using styrene-divinylbenzene-polymer-filled cartridges (500 mg, Agilent Bond Elut PPL,

https://doi.org/10.5194/egusphere-2025-6563
Preprint. Discussion started: 13 January 2026

USA), as described by Dittmar et al. (2008). In short, the cartridges were rinsed with methanol once and were soaked with methanol overnight. After draining the methanol, the cartridges were first washed with two cartridge volumes (~8 mL) of UPW, followed by two cartridge volumes of methanol, and finally with 150 mL of UPW at pH = 2. The procedure with a higher than usual pH = 2 rinse volume at the end was chosen to remove residues of the cleaning methanol. Every sample was extracted in duplicate (2 × 30 mL). To evaluate the cartridge retention capacity for DOM, the permeating sample was collected and additionally analysed for DOC. Thereafter, the cartridges were rinsed with two cartridge volumes of UPW (pH = 2) to remove remaining salts. The rinsed cartridges were dried under N_2-gas flow and DOM was eluted with 8 mL of methanol (MS-grade) into pre-combusted amber glass vials and stored in the dark at –20 °C until further analysis. DOC concentrations in the resulting SPE-DOM were determined in 1 mL aliquots which were evaporated and re-dissolved with 10 mL of UPW acidified to pH = 2. The extraction procedure was repeated with 7 UPW pH = 2 aliquots (30 mL) to acquire process blanks. Because DOC is lost during extraction, we calculate the extraction efficiency (EE) as the absolute amount of extracted DOC divided by the absolute amount of DOC introduced to the cartridge.

2.4 Molecular characterisation of DOM via ultrahigh-resolution mass spectrometry

For analysis, the carbon concentration of all DOM extracts was adjusted to approximately 2.5 ppm DOC in a 1:1 mixture of MS grade methanol and UPW. After dilution, all DOM extracts were filtered through 0.2 µm polytetrafluoroethylene polymer (PTFE) filters. Molecular analysis of DOM was conducted using ultrahigh-resolution mass spectrometry on a solariX FT-ICR-MS (Bruker Daltonik, Germany) coupled to a 15 Tesla superconducting magnet (Bruker Biospin, France). Samples were injected randomly to ensure statistically valid data acquisition using an auto-sampler (PAL3 RTC, Switzerland). The sample inlet was set to 6 µL min^{-1} at negative electrospray ionisation mode (ESI; Apollo II ion source, Bruker Daltonik, Germany), with a capillary voltage of 4 kV. Before transfer into the ion cyclotron resonance (ICR) cell, ions were accumulated in the hexapole for 0.2 s. Data acquisition was conducted in broadband mode with a scanning range of 92 - 2000 Da. Two hundred scans were accumulated for each mass spectrum. For more detailed instrument settings refer to Seidel et al (2014). *A priori*, the peak detection reproducibility and stability of the FT-ICR-MS performance were controlled by conducting duplicate measurements of each sample, and by including twenty measurements of a deep-sea DOM reference extracted from North Equatorial Pacific Intermediate Water (NEqPIW; https://uol.de/en/icbm/dsr-dom). Procedural blanks (SPE-DOM of ultrapure water acidified to pH = 2) were included for quality control of sample processing.

2.4.1 Mass spectrometry data processing

The mass spectra were internally calibrated in DataAnalysis (Version 5.0, Bruker, Germany) using a NEqPIW-based mass list of confirmed molecular formulas, achieving an averaged error margin of less than 0.1 ppm. The calibrated mass spectra were processed using the ICBM-OCEAN free processing tool to assign molecular formulas (MF) (Merder et al., 2020). In short, after defining the method detection limit (MDL), the mass spectra were recalibrated, and finally, the peaks of the individual sample mass spectra were aligned. A MDL of 3 was optimal, based on noise levels calculated from instrumental blanks and

https://doi.org/10.5194/egusphere-2025-6563
Preprint. Discussion started: 13 January 2026

peaks smaller than MDL 3 were discarded. A sample junction was conducted with a mass tolerance of 0.5 ppm. With this tolerance, a significant peak separation was achieved (Hartigan's DIP test, p = 0). For the molecular formula assignment, a mass tolerance of 0.5 ppm was applied for the following allowed elemental compositions: $C_{1\text{-}100}H_{1\text{-}200}O_{1\text{-}70}N_{0\text{-}4}S_{0\text{-}2}P_{0\text{-}1}$. Unambiguous assignment of molecular formulas was achieved across the assigned mass range (100 - 1,000 m/z), utilising stable carbon isotope confirmation and the homologous series approach (Koch et al., 2007). Based on their elemental ratios, all assigned formulas were categorised into molecular groups (Merder et al., 2020). Processing the mass spectra in ICBM-OCEAN finally yields a cross-table containing molecular formula, chemical characteristics, and sample-specific signal intensities. The cross-table was exported and prepared for further analysis.

After the MF assignment, each mass spectrum was reconstructed and inspected visually. Known contaminants were removed from the spectra. Peaks that appeared in process blank measurements with higher intensity than in the sample were removed. Only MF detected in both FT-ICR-MS measurement duplicates of each sample were considered reliable, and their intensities were averaged to produce one merged sample; signals only occurring in one of the duplicates were eliminated. Only monoisotopic species were considered as compounds; MF containing isotopologues such as ^{13}C, ^{15}N, and ^{18}O were excluded to avoid multiple counting of the same MF. The signal intensity of each identified molecular formula was normalised to the sum of the intensities of all identified molecular formulas in each sample, and normalised peak intensities were multiplied by a factor of 10,000.

2.4.2 Data analysis for FT-ICR-MS

Operationally defined compound groups, as described by Seidel et al. (2017), were used to classify the assigned molecular formulas based on their hydrogen-to-carbon (H/C) and oxygen-to-carbon (O/C) ratios. Complex DOM data is commonly classed based on elemental stoichiometries (Seidel, 2014). Those allow for assigning distinct compound groups (e.g., aromatic, unsaturated, saturated) based on their H/C-, O/C- and O/H-ratios. Where the H/C ratio can be utilised as a measure of polarity (Lechtenfeld et al., 2013; Coffey et al., 2025a), high O/H is interpreted as indicative of oxidised, carboxyl-rich material (Zark et al., 2017). We emphasise here that a molecular formula can represent millions of constitutional isomers (Hertkorn et al. 2007). Because of that, it must be considered that we do not have structural information or cannot derive the chemical functionality of a given sum formula. Although known biomolecules like carbohydrates and lipids usually have distinct elemental stoichiometries, we additionally performed FTIR analyses to verify identified compositional trends (see below). Given the high probability of newly synthesised biomolecules in the mesocosm, we added categories based on carbohydrate and lipid elemental stoichiometries and propose the terms lipid- and carbohydrate-like to account for the ambiguous nature of the interpretation, where molecular formulas may represent alternative chemical structures. That said, by categorising compounds by their elemental composition, we can provide a helpful overview of likely structures of complex organic mixtures of up to 10,000 molecular formulae.

https://doi.org/10.5194/egusphere-2025-6563
Preprint. Discussion started: 13 January 2026

In addition to exploring structural groups based on simple C, H and O elemental ratios, we calculated molecular indices that condense overall changes in the molecular composition into easily interpretable data points: (1) The modified aromaticity index (AI_{mod}), which acts as a proxy for the aromatic character of the MF, where compounds with AI_{mod} >0.5 are considered aromatics (Koch and Dittmar, 2006). AI_{mod} can be used to trace photodegradation within the DOM pool (Gonsior et al., 2009; Stubbins et al., 2010). (2) I_{bio} and (3) I_{photo}, which indicate 15 molecular formulas as markers of biological (trans-)formation and photodegradation (Bercovici et al., 2023). (4) I_{DEG}, where correlations between radiocarbon content ($\Delta^{14}C$) and FT-ICR-MS spectra were employed to develop a degradation index based on 10 single mass peaks common in marine SPE-DOM (Flerus et al., 2012). (5) A peak intensity weighted molecular lability boundary (MLB_{wL}) that defines sum formulas based on their H/C ratio as labile material (H/C ≥ 1.5) (D'Andrilli et al., 2015). Additionally, we applied a defined biomolecular classification based on molecular formula information, categorised into groups: lipid-like (O/C ≤ 0.29 & H/C > 1.6 & H/C ≤ 2.5) and carbohydrate-like (O/C > 0.6 & O/C ≤ 1.2 & H/C > 1.5 & H/C ≤ 2.5) (D'Andrilli et al., 2019; Merder et al., 2020).

Finally, we selectively traced the development of several sugar-like sum formulae, including laminaribiose ($C_{12}H_{22}O_{11}$), and five members of a related homologous series ($C_6H_{10}O_5$, $C_{12}H_{20}O_{10}$, $C_{18}H_{30}O_{15}$, $C_{24}H_{40}O_{20}$ and $C_{30}H_{50}O_{25}$). The homologous series consists of units with a mass difference of $C_6H_{10}O_5$ which corresponds to the building blocks of laminarin, a ubiquitous polysaccharide produced by marine micro- and macroalgae (Becker et al., 2020; Waska and Banko-Kubis, 2024). For readability, we present the sum of the normalised intensities of all laminarin-indicating sum formulas.

Statistical analyses and plotting were performed in R Studio (version 4.4.0, 2024, https://www.R-project.org/, Vienna Austria) using the packages ggplot2, dplyr, ggpubr, and purrr. The trend lines shown in the figures were created using Locally Estimated Scatterplot Smoothing (LOESS), a non-parametric smoothing method that employs a weighted, sliding-window average based on polynomial models to determine a line of best fit (Jacoby, 2000). The smoothing span (α = 0.5, indicating the proportion of observations used in each local regression) signifies the proportion of data points incorporated in each local fit, balancing the clarity of the trend with local variability.

2.5 Functional group characterisation of DOM via Infrared Spectroscopy

Fourier Transform Infrared (FTIR) spectroscopy was employed to analyse the functional groups in DOM. Measurements were conducted on a research-grade spectrometer (Bruker Vertex 80v), equipped with a pyroelectric detector (RT-DLaTGS) and a diamond attenuated total reflectance (ATR) cell (Bruker Platinum A225/Q). To minimise spectral contamination from atmospheric water vapor and carbon dioxide, the instrument was operated under vacuum and was purged with moisture- and CO_2-free air during sample exchange. Selected 1.5 mL duplicates of solid phase extracted-DOM covering the entire mesocosm time series were evaporated for analysis by ATR-FTIR. Each dried SPE residue was re-dissolved in 100 µL of methanol and aliquots of 4 µL were pipetted onto the ATR crystal. Following sample chamber evacuation and drying of the sample, spectra were recorded in the wavenumber range of 3800-900 cm^{-1} with a spectral resolution of 4 cm^{-1} and by averaging 100

https://doi.org/10.5194/egusphere-2025-6563
Preprint. Discussion started: 13 January 2026

interferograms, processed using Blackman-Harris 3-Term apodization function. To evaluate reproducibility and instrument stability, 3-7 repeats were conducted for each sample across multiple days. Preliminary tests with reference samples (solution of Triton-X 100, often used as a proxy for soluble surface-active organic matter (Rickard et al., 2019)) have shown that the spectral intensity variations of repeated measurements with ±30% (1σ standard deviation) were rather high, mainly caused by uneven deposition of the dissolved organic substances on the small ATR crystal. Therefore, rescaling the spectral intensity relative to the independently measured DOC content of the mesocosm samples (see below) reduced the overall scatter in the time-series data. To test for the presence of deprotonatable functional groups, such as carboxylic acid groups (Celi et al., 1997), selected samples were re-dissolved in 0.10 mM aqueous NaOH and analysed by FTIR as outlined above.

2.5.2 Data analysis of FTIR results

A typical FTIR spectrum with peak decomposition (Sadat and Joye, 2020) and peak assignment is shown in Fig. 2. The heterogeneous DOM mixture of organic compounds results in broad spectral features and pronounced overlap among the characteristic absorption bands. To improve band resolution and extract chemically meaningful information, peak decomposition was applied to the daily-averaged and baseline-corrected spectra using a peak-analyser tool (Origin 2025 Pro, Origin Lab Corporation). Based on all measured spectra, a total of 13 manually selected peak positions (see Tab. S1 in the Supplementary Information) were found to reproduce the overall spectral band shape ($0.90 < r^2 < 0.99$). Peak widths (full width at half maximum constrained to 50-500 cm^{-1}) and peak heights were used as the adjustable parameters, directly yielding integral peak intensities for further analysis. Group frequency tabulations guided peak assignments (Socrates, 2004) and literature on natural DOM analysis (Artz et al., 2008; Minor and Stephens, 2008; Abdulla et al., 2010; Pärnpuu et al., 2022), provided in Tab. S2 in the Supplementary Information. The dominant functional group signatures included a broad O–H/N–H stretch vibrational band (3700–2250 cm^{-1}), and several narrower peaks that are characteristic for C–H stretch (~2940 cm^{-1}), C=O stretch (~1730 cm^{-1}), amide I stretch (~1665 cm^{-1}), and C–O/C–O–C stretch vibrations (~1000-1200 cm^{-1}, termed C–O carbohydrate band in the following). The presence of carboxylic acids was confirmed by the comparison of DOM spectra resulting from DOM dissolved either in MeOH or NaOH (pH = 10). As shown in Fig. S1 in the Supplementary Information, a marked loss of 1730 cm^{-1} C=O band intensity, accompanied by the appearance of strong ν_{asym} (COO^-) and ν_{sym} (COO^-) bands at ~1610 and ~1370 cm^{-1}, was observed. This is characteristic of the deprotonation of COOH groups and the formation of carboxylate salts (Celi et al., 1997; Abdulla et al., 2010; Artz et al., 2008), hence indicating high fractional abundance of molecular compounds with acid functionality, presumably humic acids.

https://doi.org/10.5194/egusphere-2025-6563
Preprint. Discussion started: 13 January 2026

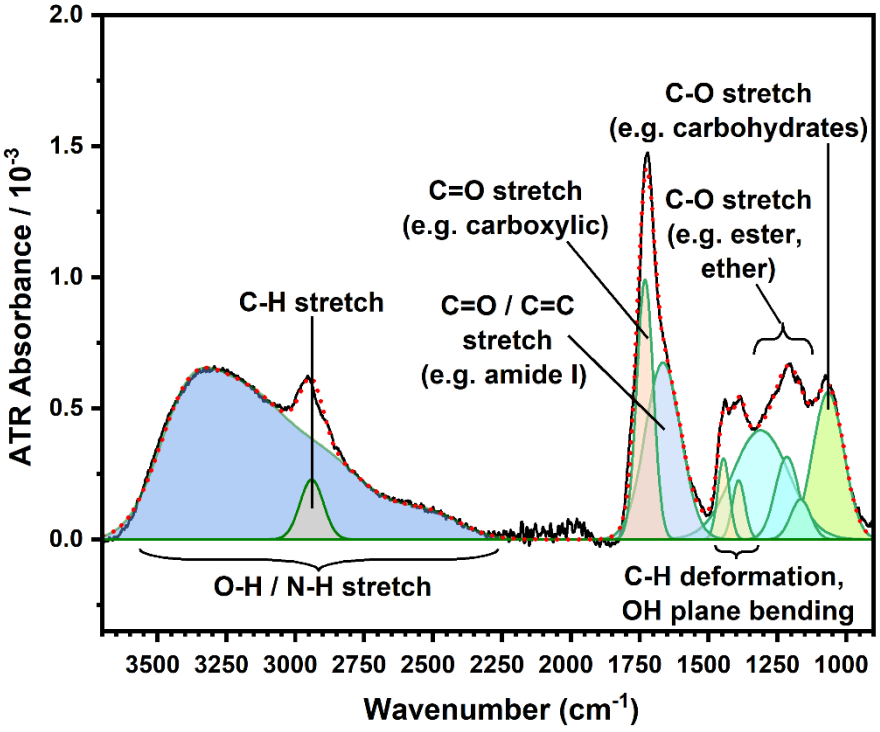

Fig. 2: ATR-FTIR spectrum decomposition, resolved into 13 individual peaks using a multiple-peak Gaussian fitting routine. Note that the broad O–H/N–H stretching vibrations envelope was deconvoluted into four components, but is displayed here as a single composite band.

Following spectral decomposition, band areas were quantified by integration. For time-series analysis, the integrated intensity I_{raw} was further normalised with respect to variations in the water volume used for extraction, V_{sample}, and by re-scaling the FTIR intensity to the measured, more reliable DOC content m of the corresponding sample extract. This was accomplished by a mass-balance correction factor I_C/m, where I_C was taken as the total integral of carbon-containing functional group peaks. Accordingly, the ratio I_C/m represents the average IR intensity in a given sample spectrum per unit carbon mass in the corresponding extract. Fig. S2 in the Supporting Information shows that I_C scales linearly with m ($r = 0.96$), so I_C/m serves as a re-scaling factor to account for the variability in the sample loading of the sample on the ATR crystal. The resulting signal, $I = I_{raw} \times (V_{sample})^{-1} \times (I_C/m)^{-1}$, enables robust inter-sample comparison and is represented as a normalised I_{norm} signal in the trend graphs, by dividing I by the maximum value within the respective time series. To examine patterns in functional group abundances, a trend line was generated using the same LOESS script used for the FT-ICR-MS data. The smoothing span was adjusted from $\alpha = 0.50$ to 0.75 to account for the reduced number of data points.

https://doi.org/10.5194/egusphere-2025-6563
Preprint. Discussion started: 13 January 2026

3 Results

3.1 Physicochemical and biogeochemical properties of the mesocosm

The 33-day mesocosm study, carried out from late spring to early summer 2023, was marked by notable seasonal warming mainly under clear and dry conditions, along with an increase in salinity from 29.2 to 32.3 (Bibi et al., 2025). The daily average surface temperature rose from 16°C in late spring to a peak of 23°C in early summer, with daily fluctuations of up to 7 °C. Solar irradiance peaked in early June, with intermittent rainfall and cloud cover causing brief reductions in radiation and air temperature. Albedo remained low (~4-5 %) throughout May, then increased sharply in early June, coinciding with high concentrations of reflective coccoliths at the surface. Chl*a* concentrations increased during the experiment (Fig. 3), determined by FerryBox (PocketBox, 4H-Jena, Germany). Bibi et. al (2025) observed three phases based on Chl*a* levels: a *pre-bloom* phase with low concentrations (~2 mg L^{-1}, May 18-26) a *bloom* phase with elevated concentrations (~14 mg L^{-1}, May 27-June 4), and a *post-bloom* phase during which Chl*a* declined (~3 mg L^{-1}, June 5-16).

During the mesocosm, two consecutive phytoplankton blooms were observed. The first bloom at the end of May, was dominated by the coccolithophore *Emiliania huxleyi*, as identified via electron microscopy, and was associated with elevated chlorophyll *c* concentrations. The particle size distribution during this period corresponded to the average size of *E. huxleyi* cells (5-10 µm). The second bloom, occurring in early June, was dominated by the diatom *Cylindrotheca closterium*, as confirmed by FlowCam and conventional microscopy. After the bloom phases, phytoplankton biomass declined, while turbidity and albedo remained elevated (Bibi et al., 2025).

3.2 Quantitative parameters: DOC, TDN, DON, Enrichment Factor (EF) and Extraction Efficiency (EE)

The development of various quantitative and qualitative DOM parameters during the mesocosm study can be categorised into three distinct behavioural types: (1) consistent increase or decrease, suggesting the parameter changes at a steady rate, either in both SML and ULW or within each individual water mass; (2) abrupt increase or decrease, indicating a change specific for one of the three phases; and (3) growing SML compartmentalisation, where the parameter shows more pronounced development in the SML compared to the ULW.

DOC concentrations and the DOC/DON ratio in the SML compartmentalised in tandem with the increase of Chl*a* during the bloom phase (Fig. 3 a,d; Tab. 1). Throughout the bloom, SML DOC was enriched compared to ULW, despite an overall increase in the ULW DOC (EF, Fig. 3 e). This enrichment increased drastically during the bloom and the post-bloom phase. Both SML and ULW maintained high DOC concentrations after the bloom, despite Chl*a* levels dropping in the post-bloom phase.

TDN concentrations abruptly decreased in the SML and ULW at the start of the bloom phase (Fig. 3 b) with higher values in the SML throughout the study. During the post-bloom phase, TDN in the SML decreased while the ULW TDN remained

https://doi.org/10.5194/egusphere-2025-6563
Preprint. Discussion started: 13 January 2026

335 relatively stable throughout the whole study. DON showed an immediate increase in SML compartmentalisation compared to the ULW. DON concentrations increased in the SML as well as in the ULW during the pre- and bloom phases (Fig. 3 c). DON reached its maximum levels in both the SML and ULW at the start of the bloom phase, before declining until the end of the study. During the bloom and post-bloom phases, DON levels fell in the SML. The decline led to a convergence in DON levels between SML and ULW.

340

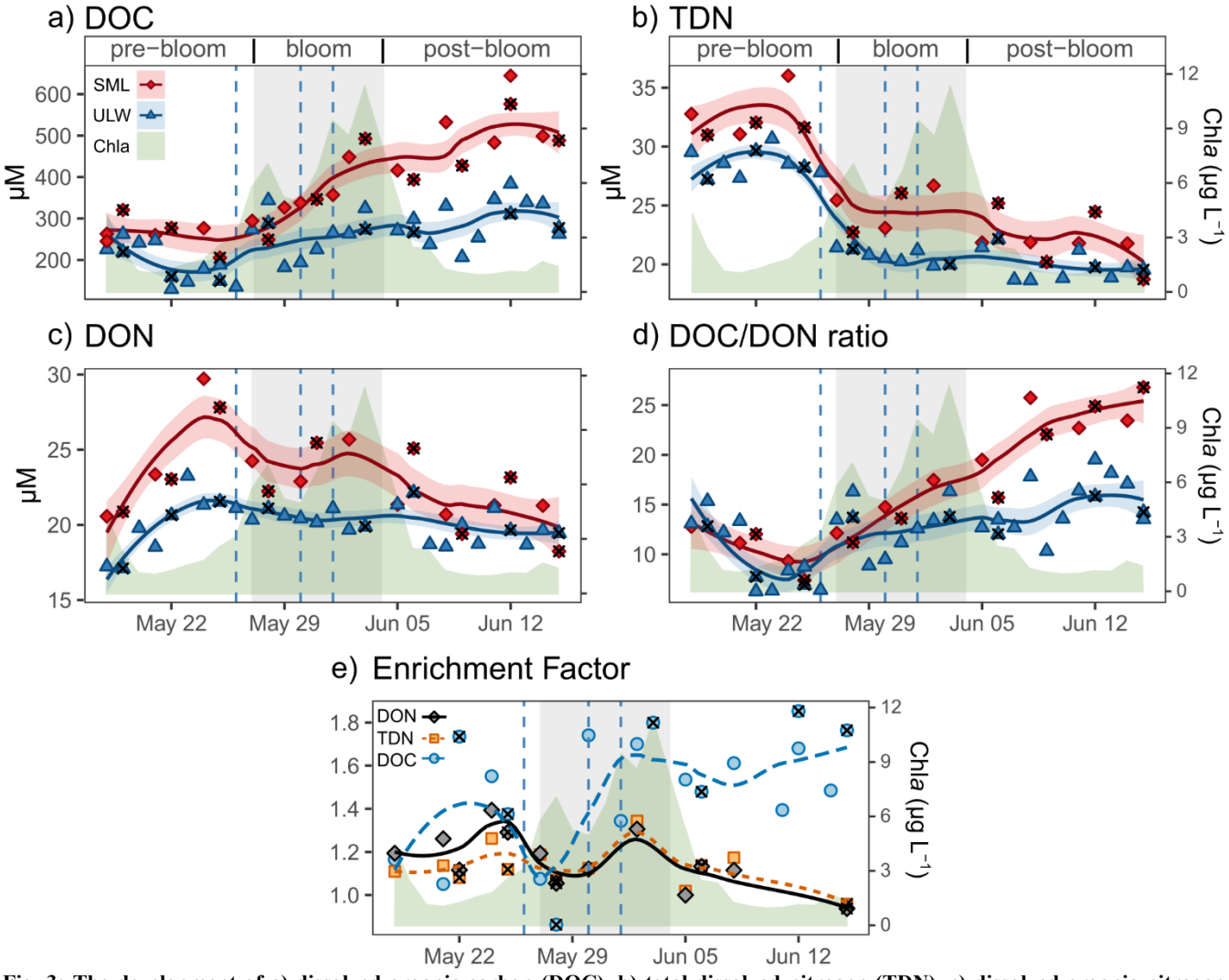

Fig. 3: The development of a) dissolved organic carbon (DOC), b) total dissolved nitrogen (TDN), c) dissolved organic nitrogen (DON), and d) the DOC to DON ratio during the mesocosm study. Chl*a* development is shown in green shading. Red indicates SML (sea surface microlayer), blue indicates ULW (underlying water). The blue vertical dotted lines indicate the dates of nutrient
345 **addition. Black cross marks the polycarbonate (PC) filter, with glass fibre (GFF) as the default (including GMF for DOC and GD/X for TDN). e) Development of enrichment factor (EF = concentration$_{SML}$/concentration$_{ULW}$) of DOC, DON, TDN over the course of the mesocosm study. The trend lines were generated using Locally Estimated Scatterplot Smoothing (LOESS). The shaded area around the curve represents the 95% confidence interval.**

https://doi.org/10.5194/egusphere-2025-6563
Preprint. Discussion started: 13 January 2026

3.3 Temporal changes and SML/ULW comparison in DOM composition

The index for bioproduction (I_{bio}) and the weighted average of the H/C ratio showed a consistent increase throughout the mesocosm study in both the SML and ULW (Fig. 4 a, f, Tab. 2). Meanwhile, the indices for (bio-)degradation (I_{DEG}, where lower values indicate less degraded DOM) and the index for photodegradation (I_{photo}, where lower values indicate greater photodegradation) decreased consistently (Fig. 4 c, l). The same decreasing trend was shown by the aromaticity index (AI_{mod}) and the weighted average (w.a.) of highly unsaturated sum formulas (H.U with AI_{mod}>0.5, Fig. 4 g, m). None of the abovementioned parameters showed a clear trend of increasing SML compartmentalisation.

In contrast, increasing SML compartmentalisation was noticed for the intensity weighted molecular lability boundary (H/C > 1.5, MLB_{wL}), the humic-like fluorescent DOM (FDOM), and finally the w.a. of carbohydrate-, lipid- and protein-like fractions of the DOM pool (Fig. 4 b, h, i, k, Tab. 2). The compartmentalisation was distinct and consistent despite a concurrent overall increase in the ULW (e.g. in the MLB_{wL}, Fig. 4 b), or overall decreases in both, SML and ULW (e.g. FDOM, Fig. 4 k). Specifically, in the SML, the sum of the normalised intensities of laminarin indicating formulas increased abruptly in the SML during the bloom phase (Fig. 5). In contrast, the ULW showed only sporadic appearances of the sugar-like formulas, with relative intensities remaining below or only slightly above the method detection limit throughout the study, similar to conditions in the SML before the bloom. Furthermore, these formulas showed a diurnal trend, where samples taken before sunrise had higher laminarin-like signal intensities than those taken in the afternoon.

The SPE-DOC/SPE-DON and O/H ratios showed no notable trends in the ULW (Fig. S4 a, b). While both parameters increased in the SML after the bloom, the latter decreased during the pre-bloom phase, reaching the lowest values in the middle of the bloom phase. Finally, the O/H ratios increased during the second half of the bloom phase, peaking at the beginning of the post-bloom phase before decreasing again until the end of this phase.

The DOC extraction efficiency (EE) was consistently at least 20% lower in the SML than in the ULW samples and decreased during the bloom phase in both the SML and ULW, before returning to pre-bloom levels during the post-bloom phase. Conversely, permeating DOC (per-DOC) was consistently higher in the SML than in the ULW (Tab. 1). During the bloom phase, per-DOC increased in the SML until the end of the mesocosm study, while in the ULW it decreased, especially during the bloom. The recovery budget (total; $n_{DOC} \approx n_{EE} + n_{per\text{-}DOC}$) for per-DOC and EE only approached 100% for the ULW in the pre-bloom and post-bloom phases (Tab. 1). Meanwhile, the recovery budget for the SML and during bloom ULW indicated that 10-20% of DOC remained attached to the PPL cartridge during extraction and was not recovered during elution. Despite the loss of DOC during PPL extraction, the SPE-DOC/SPE-DON ratios were consistently higher in the SML than in the ULW both before and after the bloom (Fig S4 a).

https://doi.org/10.5194/egusphere-2025-6563
Preprint. Discussion started: 13 January 2026

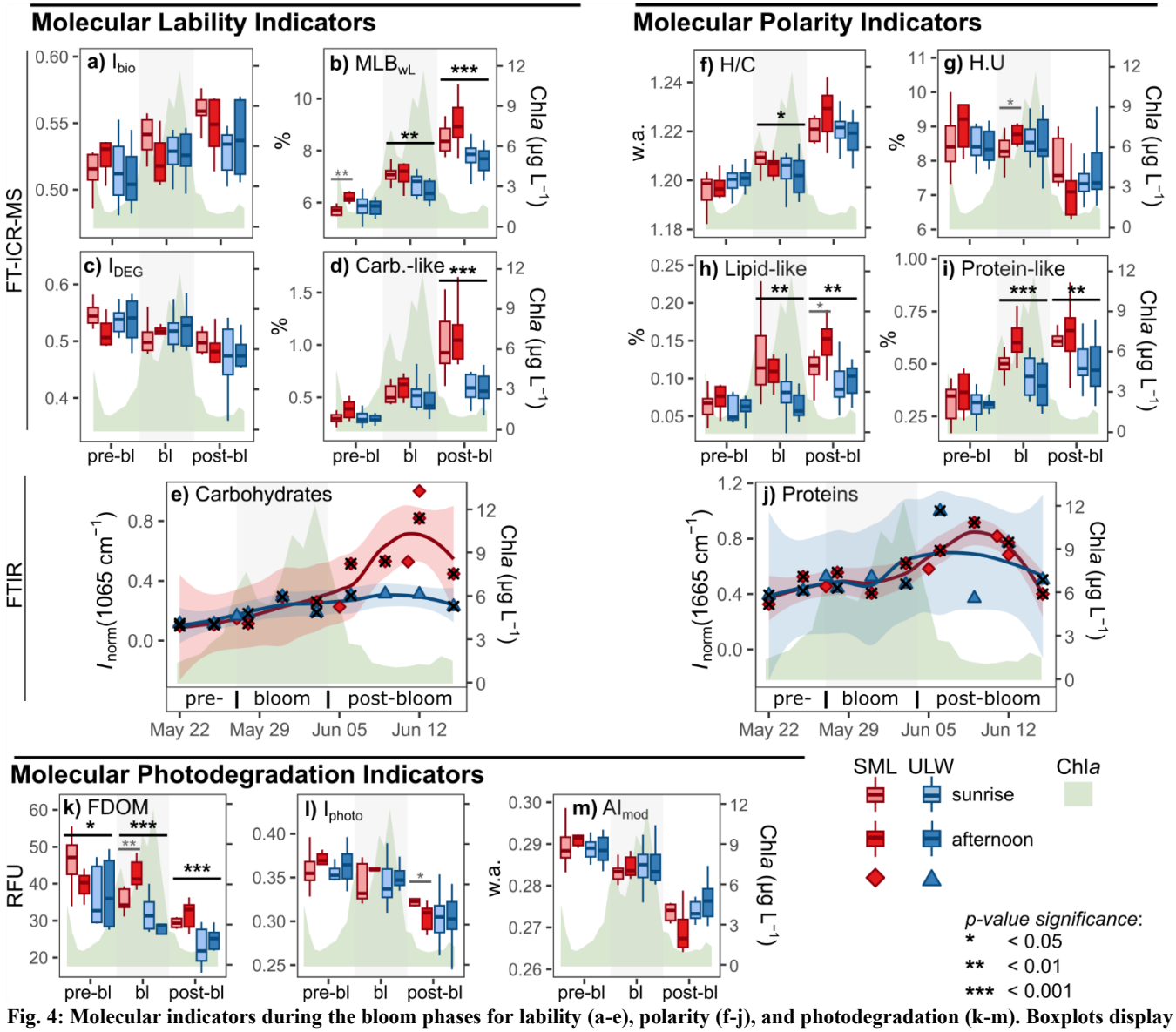

Fig. 4: Molecular indicators during the bloom phases for lability (a-e), polarity (f-j), and photodegradation (k-m). Boxplots display FT-ICR-MS data, while smoothed scatter plots show characteristic FTIR vibrational data. SML in red, ULW in blue, sunrise in desaturated, afternoon in saturated colour; the green area indicates Chl*a* development; black cross marks the polycarbonate filter, with GFF as the default.

https://doi.org/10.5194/egusphere-2025-6563
Preprint. Discussion started: 13 January 2026

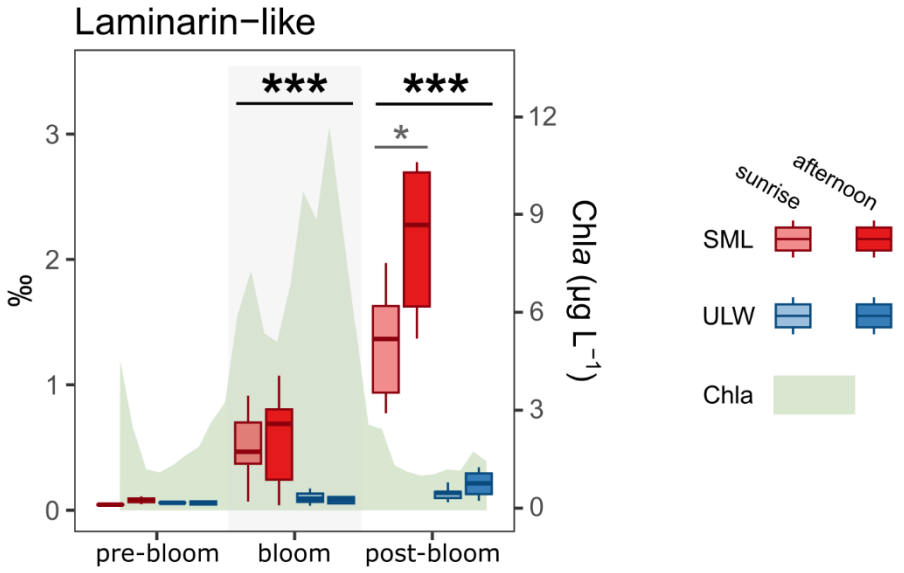

Fig. 5: The normalised intensities of molecular formulas indicative of laminarin are expressed in parts per ten thousand (‰). These trends for the pre-bloom, bloom, and post-bloom phases in the SML sunrise and afternoon samples show an abrupt increase and greater compartmentalisation during and especially after the bloom. Note the diurnal trend in the post-bloom phase, which indicates higher laminarin production during the day. Meanwhile, only a slight increase in laminarin-related sum formulas was detected in the ULW.

3.3 Changes in structural patterns of the DOM composition

The pronounced increase of carbohydrate-like formulae in the bloom and post-bloom SML was strongly supported by the supplemental FTIR measurements. Fig. 6a and b show FTIR spectra for SML and ULW samples, averaged over the three phases of the phytoplankton bloom development. For spectral assignment, refer to Fig. 2 in section 2.5.2 and Tab. S2 in the Supplementary Information. During the pre-bloom phase (pink-coloured spectrum) and bloom phase (green), the overall spectral profile and thus also the relative abundances of functional groups remained largely unchanged . However, in the post-bloom phase (wine colour), substantial spectral alterations were evident, notably a strong enhancement in the relative intensities of the spectral features associated with the broad O–H/N–H band (~3700-2500 cm^{-1}), the aliphatic C–H (3025-2785 cm^{-1}), and the C–O/C–O–C region (~1170–940 cm^{-1}). These changes were much more pronounced in the SML samples and are indicative of a sudden increase and compartmentalisation of monomeric carbohydrates and/or polysaccharides during the post-bloom phase.

In particular, the vibrational band around 1065 cm^{-1} is well known as a characteristic peak for carbohydrate-like molecular structures (Artz et al., 2008; Minor and Stephens, 2008; Abdulla et al., 2010; Pärnpuu et al., 2022). The absolute carbohydrate signal trend (in terms of I_{norm}) shown in Fig. 4 e indicated an increase both in the ULW and SML during the pre-bloom and bloom phases, but it was much more pronounced in the SML in the post-bloom phase. Both the timing of the carbohydrate abundance as well as the maximum, about three times enrichment in the SML were consistent with the data on carbohydrate-like sum formulas from FT-ICR-MS shown in Fig. 4 d. The substantial share of carbohydrate-like substances in the post-bloom

https://doi.org/10.5194/egusphere-2025-6563
Preprint. Discussion started: 13 January 2026

SML samples was also evident in the relative spectral trends (in terms of the ratio I/I_C, see Fig S5 a in the Supplementary information). Here, the relative spectral contribution of the integrated 1065 cm^{-1} band with respect to the total integral of carbon-containing functional groups was increasing from about 10% to 30% over the course of the mesocosm experiment in the SML but remained almost constant in the ULW within the scatter of the data.

Table 1: Average dissolved organic carbon (DOC) concentrations in the sea surface microlayer (SML) and underlying water (ULW) before and after solid phase extraction (SPE), as well as in the permeated sample (per-DOC) during the three distinct bloom phases. The per-DOC/DOC ratio reflects the proportion of DOC not retained by the SPE resin. Extraction efficiency (EE) indicates the relative amount of carbon recovered after SPE (i.e., retention plus elution). The last row (total) represents the total fraction of DOC recovered either by SPE extraction or per-DOC.

	pre-bloom			bloom			post-bloom		
	SML	**ULW**	**t-test / p-value**	**SML**	**ULW**	**t-test / p-value**	**SML**	**ULW**	**t-test / p-value**
DOC	264 µM (±34 µM), n=7	190 µM (±46 µM), n=12	0.0014 **	365 µM (±76 µM), n=9	261 µM (±50 µM), n=11	0.0051 **	485 µM (±82 µM), n=7	301 µM (±51 µM), n=13	<0.001 ***
per-DOC	119 µM (±72 µM), n=14	98 µM (±51 µM), n=22	0.17	178 µM (±71 µM), n=17	143 µM (±106µM), n=18	0.44	217 µM (±52 µM), n=16	122 µM (±55 µM), n=30	<0.001 ***
per-DOC / DOC	40% (±12%), n=12	46% (±23%), n=22	0.33	49% (±13%), n=16	34% (±22%), n=16	0.034 *	45% (±13%), n=14	41% (±16%), n=22	0.38
EE	52% (±14%), n=8	62% (±10%), n=10	0.13	36% (±11%), n=8	49% (±20%), n=11	0.1	48% (±16%), n=7	59% (±12%), n=16	0.13
total	93% (±19%)	108% (±25%)	/	85% (±18%)	83% (±30%)	/	93% (±21%)	100% (±21%)	/

p-value significance: * (< 0.05), ** (< 0.01), and *** (< 0.001)

We also investigated trends in various peak integrals and peak integral ratios to identify possible changes in the overall polarity of DOM in the SML and ULW. In particular, the peak ratio of the C–H/C=O, CH/(amide I), C–H/(O–H/N–H), and C–H/(C–O/C–O–C) stretch bands may indicate changes in the polarity resulting from the mix of different compound classes with varying C/H/O/N content. Note that lipids with long alkyl chains may have contributed disproportionately to the C–H signal. The C=O signal was confirmed to have a strong component of carboxylic acid functionality (Fig. S1), the amide I band is indicative of proteins, and the C–O/C–O–C band is attributed to carbohydrates. Corresponding ratio plots are provided in Fig. S9 in the Supplementary Information, together with the spectral trends for the C–H, O–H/N–H, and C=O bands in Fig. S6, S7, S8. The absolute spectral trends all showed a significant increase in the SML similar to that observed for the carbohydrate

https://doi.org/10.5194/egusphere-2025-6563
Preprint. Discussion started: 13 January 2026

band at 1065 cm^{-1}. Carbohydrates are expected to give absorption changes in the order C–O/C–O–C > C-H ≈ O–H > C=O, where significant effects on the C=O band are only seen if uronic acids, acetylated, or esterified polysaccharides are present. Hence, the observed weak trends in the ratio plots were all consistent with carbohydrate enrichment in the SML. As expected, the CH/(C–O/C–O–C) ratio was slightly decreasing, the ratios C–H/C=O and C–H/(O–H/N–H) were mostly constant, and the CH/(amide I) ratio increased, the latter because the amide I band is not affected by carbohydrates. Finally, the absolute and relative intensity trends of the 1665 cm^{-1} amide I stretch vibration peak of proteins are shown in Fig. 4 j and Fig. S5 b. Again, we resolved a significant signal increase towards the post-bloom phase, in reasonable agreement with the FT-ICR-MS data on protein-like formulas shown in Fig. 4 i. However, unlike the relative trends for the C-H, O-H/N-H, and C=O bands, which may all include signal contributions from carbohydrates, the relative spectral contribution of the protein band decreased significantly in the SML but remained constant in the ULW.

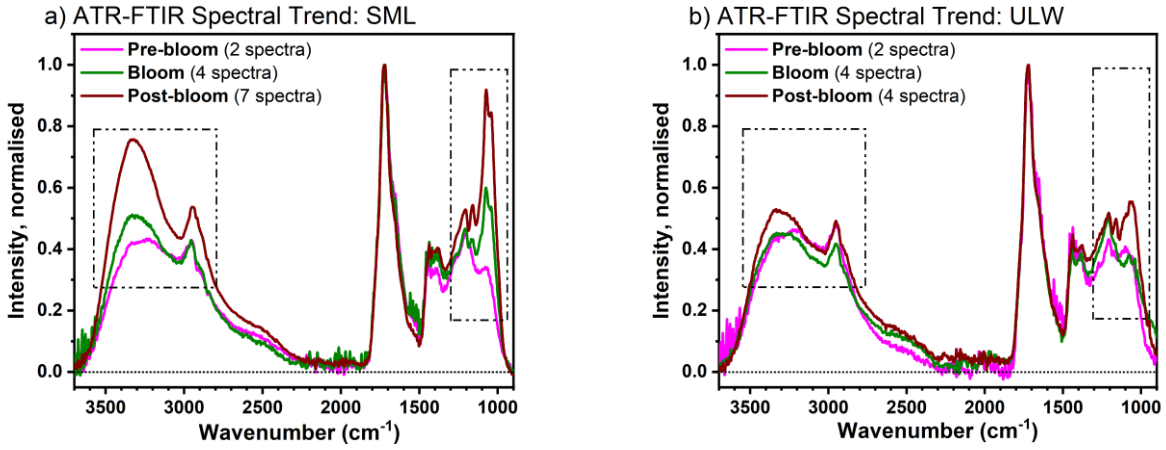

Fig. 6: FTIR spectral trends for pre-bloom, bloom, and post-bloom phases for (a) the SML (revealing significant spectral changes) and (b) the ULW (revealing unaltered spectra). To allow direct comparison of the overall spectral shape, all spectra are normalised to the peak intensity of the intense carbonyl band at 1730 cm^{-1}.

4 Discussion

Studying the low molecular weight fraction of DOM in the SML during phytoplankton blooms remains a challenge due to the difficulty of sampling the dynamic SML and the complexity of its molecular composition. Nonetheless, based on our FT-ICR-MS and ATR-FTIR data, we identified carbohydrate-like material as the primary contributor to DOM in the SML, during and after phytoplankton blooms. Also, lipid- and protein-like formulas appeared to increase in the SML spectra obtained by FT-ICR-MS, but potential FTIR lipid signatures were obscured by stronger spectral changes associated with carbohydrate enrichment. We will examine how the conclusions derived from our experimental findings correspond to our original

https://doi.org/10.5194/egusphere-2025-6563
Preprint. Discussion started: 13 January 2026

hypotheses regarding (1) photosynthetic bioproduction pathways, (2) polarity-driven accumulation of organic matter, and (3) photo- and biodegradation patterns in SML and ULW. Lastly, the implications of our findings for a better understanding of SML organic geochemistry in natural environments will be discussed.

4.1 Bioproduction of buoyant particles drives the accumulation of carbohydrate-like DOM in the SML

We observed a strong accumulation of up to 600µM DOC in the SML with an elevated DOC/DON ratio after the bloom (Fig. 3) that exceeded the Redfield ratio, suggesting in situ carbohydrate production (Hammer and Kattner, 1986; Van Den Meersche et al., 2004). In contrast, initial DOC concentrations in our mesocosms had matched natural summer levels in the North Sea (~ 210µM cf. Böttcher et al., 1998; Seidel et al., 2015), confirming realistic starting conditions. Over the course of the mesocosm, we observed a decrease in extraction efficiency (EE) and an increase in permeated DOC (per-DOC) (Tab 1), both suggesting a shift towards a less extractable, more polar DOM pool, since retention on the PPL-SPE sorbent decreases with an increase in polarity of organic compounds (Raeke et al., 2016). In addition, elevated O/H-ratio also indicated a more polar molecular composition, reflecting an increased abundance of oxygen-containing functional groups such as carboxylic acids (Zark et al., 2017; Fig S4 b). A high abundance of compounds with carboxyl functionality was also detected by FTIR measurements, which tested the effects of either methanol or alkaline water (pH = 10) on proton-binding sites in DOM (Fig. S1).

Moreover, the molecular FT-ICR-MS data (Fig. 4 a, b and Tab. S3) indicated the accumulation of bioavailable compounds through an increased MLB_{wL} (D'Andrilli et al., 2015) and I_{bio} (Bercovici et al., 2023). Most notably, the intensities of carbohydrate-like molecular formulas clearly increased, especially in the SML after the bloom. This was also supported by the FTIR data, where both absolute and relative carbohydrate-related spectral signatures were strongly enhanced while the fraction of proteinaceous material diminished (Figs. 4 e, j, S5. This is best seen in the characteristic carbohydrate-indicating peak at 1065 cm^{-1}, which showed a 6-fold increase in the absolute spectral contribution and a 3-fold increase in the relative spectral contribution (Fig. 4 e). By combining FTIR and FT-ICR-MS data, we could show that carbohydrate-like substances get strongly enriched in the overall carbon pool, forming the main component of the sudden DOC increase observed in the SML during the bloom and post-bloom phases. This observation also aligns with data presented by Bibi et al. (2025) for the same mesocosm experiment, which reported a shift in microbial substrate utilisation towards carbohydrates during the later stages of the bloom, especially in the SML (Fig. 7 f in Bibi et al., 2025).

Note that we did not detect the sum formulas of monosaccharides like glucose ($C_6H_{12}O_6$) which can be measured with targeted methods like HPLC (Barthelmeß and Engel, 2022), and which were previously found by our group in FT-ICR-MS spectra of macroalgal beach wrack DOM (Waska and Banko-Kubis, 2024). PPL-SPE has low recoveries for carbohydrates (Raeke et al., 2016), and FT-ICR-MS relies solely on sum formulas for molecular identification which restricts the differentiation of structural isomers, making it harder to assign chemical functionality (Merder et al., 2020). Despite these limitations, it is

https://doi.org/10.5194/egusphere-2025-6563
Preprint. Discussion started: 13 January 2026

especially noteworthy that we observed a selective accumulation of carbohydrate-like DOM in both our FT-ICR-MS and FTIR measurements. The combination of FTIR and FT-ICR-MS in our study enabled us to reveal the prevalence of sugar-like compounds that cannot be captured by conventional targeted methods but show similar elemental stoichiometries and indicate similar environmental behaviour, with rapidly increasing signal intensities during and after the bloom, strong enrichment in SML samples, and absence in pre-bloom samples and our deep-sea reference NEqPIW (Fig. 5). Our findings demonstrate that more information about the sources and quality of early diagenetic DOM can be obtained from untargeted FT-ICR-MS and FTIR data than one might expect. For example, the detected laminarin-like formulae could originate from polysaccharides secreted by diatoms, which commonly include glycans like laminarin. These serve as essential energy metabolites microalgae (Becker et al., 2020; Biersmith and Benner, 1998). In our mesocosm experiment, they were found in the SML and displayed a significant diurnal pattern, likely because of overshoot laminarin production within diatom cells during daylight (Becker et al., 2020). Moreover, the increasing laminarin-like formulas appeared mainly in the SML but were barely detectable in the ULW, suggesting that the SML is a hotspot for *in situ* production or increased biological and abiotic (photo-)degradation of high molecular-weight DOM and POM during the day (Kitaoka et al., 2012; Kumagai et al., 2014; Kim et al., 2018). In addition, a broader carbohydrate-like compound class was identified which showed a similar if slightly weaker trend. We suggest that this hidden group of sugar-like compounds extends well into the so far still poorly characterised DOM geometabolome and may provide a crucial spatiotemporal link between known and -yet- unknown molecular building blocks.

As an additional line of evidence, our observed accumulation of nitrogen-depleted DOC in the SML (Fig. 3 a, c, d) during and after the phytoplankton bloom is in accordance with previous reports and typically attributed to carbohydrate stress release (Ittekkot et al., 1981; Grossart et al., 2007; Laß et al., 2013; Thornton, 2014; Engel et al., 2017). Long-chain polysaccharides are produced by the overflow production of the present microalgae: *Emiliania huxlei* and *Cylindrotheca closterium*. While the observed succession, with *E. huxleyi* preceding *C. Closterium*, diverges from the canonical North Sea sequence where diatoms typically bloom first, both taxa are characteristic of the regional summer flora (Balch et al., 1992; Weeks et al., 1993; Malviya et al., 2016). Their presence confirms that the mesocosm community, though influenced due to pre-filtration and elevated temperatures (up to 24 °C), remained ecologically representative of North Sea dynamics. These species are known for producing polysaccharides that serve as energy storage and provide UV protection for the algae during periods of high UV stress or nutrient depletion towards the end of the bloom phase (Lavaud et al., 2004; Van Oostende et al., 2013; Scholz et al., 2014; Thornton, 2014). The lack of available nitrogen at late bloom stages hinders the synthesis of essential proteins and nucleic acids, which are necessary to shut down the photosynthetic apparatus (Thornton, 2014). When the cell's carbohydrate storage capacity is exceeded, excess organic carbon is expelled into the surrounding environment. Since light and inorganic carbon were readily available in the SML, this strategy imposes little to no cost on the phytoplankton (Wood and Van Valen, 1990; Underwood et al., 1999).

https://doi.org/10.5194/egusphere-2025-6563
Preprint. Discussion started: 13 January 2026

This raises the question of whether the accumulating DOM is produced in situ through photosynthetic and autotrophic processes in the SML (Goes et al., 1996; Thornton, 2014), or is transported up from the ULW in by previously formed buoyant POM that aggregates at the surface and is then degraded into DOM (Carlson, 1993; Chin et al., 1998; Passow, 2002). The filters for SML and ULW samples showed a high particle load after the bloom (Fig. S3). In line with our observations, Bibi et al. (2025, Figure 6) reported a high POC and PON occurrence in the ULW during the bloom and a decrease in POM concentration in the post-bloom phase of the mesocosm study. The high abundances of POM could directly influence DOM dynamics because POM and DOM can be transformed into each other through reversible processes (Chin et al., 1998; Passow and Engel, 2001; Passow, 2002; Silva et al., 2025): DOM can be generated from POM by microbial degradation (Corzo et al., 2000; Passow, 2002; Wurl et al., 2011), as well as abiotic photolysis and leaching (Chin et al., 1998; Passow, 2002; Ortega-Retuerta et al., 2009; He et al., 2016). On the other hand, DOM – especially long-chain polysaccharides – can form POM by spontaneous self-assembly (Chin et al., 1998; Passow, 2002), and shear- or turbulence-induced coagulation, particularly on the ocean surface, where high shear forces cause entanglement (Logan et al., 1995; Passow, 2000; Engel and Passow, 2001). The entanglement of long-chain carbohydrates into high buoyancy, surface-active POM transports OM into the SML up from the ULW, where the POM, again, can be transformed in situ to DOM (Mopper et al., 1995; Zhou et al., 1998; Passow and Engel, 2001).

Towards the end of the study, an observed increase in microbial carbohydrate utilisation (Bibi et al., 2025) led us to expect indications of the biological transformation and degradation of the accumulated carbohydrate-like DOM (Moran and Zepp, 1997; Koch et al., 2014; Bercovici et al., 2023). An increase in EE in both the SML and ULW towards the end of the study showed that labile, polar, and bloom-derived DOM was progressively degraded and became increasingly refractory (Tab. 1). Nonetheless, the I_{DEG}, which reflects the degree of bacterial degradation (Flerus et al., 2012), showed no notable change throughout our study. This may suggest that the study duration was too short to capture the impact of slow-acting degradation processes indicated by I_{DEG}. Considering the elevated DOC/DON- and H/C- ratio (Figs. 3 d, 4 f), I_{bio} (Fig. 4 d), and the trends in carbohydrate-like DOM (Fig. 4 d), it appears that we observed an extended phase of labile and polar DOM production, despite the Chl*a* decrease, hence, without phytoplankton growth. This points towards a lagged degradation of accumulated POM in the SML into DOM, with not enough time to remineralise the labile DOM fractions until the end of the mesocosm study (Kepkay et al., 1997).

4.2 Phytoplankton blooms favour the accumulation of polar amphiphilic DOM in the SML

While some studies highlight buoyancy-driven enrichment of DOM in the SML (Engel and Passow, 2001; Wurl et al., 2011), others point to lipophilic compounds preferentially accumulating at the air-sea interface (Carlson and Mayer, 1980; Cunliffe and Murrell, 2009; Lechtenfeld et al., 2013). This accumulation can be seen as a phase separation, where molecules with higher hydrophobicity (e.g., aromatics) or hydrophobic groups (e.g., lipids) concentrate at the surface because they are energetically unfavourable in the salty ULW, which exhibits strong polar interactions between water and salt ions (‘salting out’)

https://doi.org/10.5194/egusphere-2025-6563
Preprint. Discussion started: 13 January 2026

(Setschenow, 1889; Xie et al., 1997). We observed an increase in H/C ratios alongside a decrease in the modified aromaticity index (AI_{mod}), indicating that the SML was not enriched in refractory aromatic compounds but rather in fresh, aliphatic components (Fig. 4 f, g, m). This change suggests a dilution of the refractory natural seawater background by labile, bloom-derived DOM, coupled with further photobleaching of aromatic components at the interface (discussed below).

To characterise these aliphatic surfactants within the SML, we distinguished between dry and wet surfactants based on their H/C and O/C ratios. Dry surfactants, such as lipid-like compounds, possess high H/C and low O/C ratios; their insoluble, lipophilic nature drives strong preferential accumulation at the air-water interface (Frew et al., 2006). Conversely, wet surfactants (e.g., protein- and carbohydrate-like formulas) exhibit higher O/C ratios, which renders them water-soluble while still maintaining their surface activity. Notably, the stoichiometry of the protein-like fraction closely resembles that of Triton X-100, a standard synthetic surfactant, supporting the use of protein-like DOM as a molecular proxy for surface activity (Rickard et al., 2019). We observed that lipid- and protein-like compounds significantly enriched in the SML (Fig. 4 h, i). Although molecular stoichiometry alone cannot fully resolve the structural and steric properties that define amphiphilic surfactants, the observed temporal patterns of these compounds track the diagenetic state of the bloom, suggesting their ecological appearance is a robust indicator of surface-active material.

Our data confirm that during phytoplankton blooms, SML-DOM composition is heavily influenced by resident algal species, and mainly consists of carbohydrates (Fig. 3 d, Fig. 4 a - e) with smaller amounts of lipids and proteins (Fig. 4 h, i, j) (Myklestad, 1995; Croot et al., 2007). As previously discussed, carbohydrates constitute the majority of accumulated organic matter due to "overflow production" typical of late-stage phytoplankton blooms (Thornton, 2014). Our observations are in contrast with previous studies: Although carbohydrates can build up because of buoyancy and may function as wet surfactants, likely in the form of lipopolysaccharides (Laß, 2011), their role in forming the interfacial surfactant layer surface layer is considered secondary compared to more surface-active species (Elliot et al., 2018; Asmussen-Schaefer, 2025). The observed dominance of carbohydrate signals during FTIR analysis made it difficult to draw conclusions about more subtle distribution patterns of other, non-carbohydrate compounds. However, FT-ICR-MS analysis enabled us to identify abundance trends of the minor lipid- and protein-like fractions (Fig. 4h,i) that mirrored those of the carbohydrate-like compounds. Since lipid- and protein-like fractions tend to be preferentially accumulated at the interface owing to their specific polarity and high surface activity, they could have a disproportionate effect on the physical properties of the interface and on air-sea gas exchange, despite contributing less to the total DOM mass. This observation aligns with the high surfactant coverage reported by Bibi et al. (2025) and Asmussen-Schaefer et al. (2025), as well as earlier findings of lipid accumulation in slick waters (Frew et al., 2006). Therefore, our molecular data indicate that the enrichment of DOM in the SML results from a complex interaction of buoyancy and polarity-driven chemical phase separation. Furthermore, considering their high energy yield as a substrate for microbes, carbohydrates likely are preferentially utilised, making a shift from “carbo-SML” to “lipid-SML” conditions in the wake of phytoplankton blooms a likely scenario under natural conditions.

https://doi.org/10.5194/egusphere-2025-6563
Preprint. Discussion started: 13 January 2026

4.3 Photodegradation of DOM affects SML and ULW in the same way

This mesocosm study was conducted at the transition from late spring to early summer in Northern Germany in the northern hemisphere (Bibi et al., 2025). During this time, the DOM-enriched SML was directly exposed to intense solar radiation, making it a potential hotspot for photochemical reactions (Wurl and Holmes, 2008; Engel et al., 2017; Jibaja Valderrama et al., 2025). These high irradiation conditions, compared to deeper water masses, were expected to alter the DOM composition (Miller and Moran, 1997; Bercovici et al., 2023). We saw photodegradation in both SML and ULW, which was evident through a significant decline in the modified aromaticity index (AI_{mod}) during the mesocosm (Fig. 4 m), indicating photobleaching of aromatic compounds (Stubbins and Dittmar, 2015). This trend was also supported by the concurrent decrease in humic-like fluorescent FDOM (Fig. 4 k), likely due to the UV-induced breakdown of aromatic structures and a loss of chromophores and, subsequently, fluorescent properties of DOM (Allard et al., 1994; Moran et al., 2000). The I_{photo}, which captures cumulative photochemical alteration, followed the same downward trend in both the SML and ULW (Fig. 5 l), indicating loss of photosensitive compounds from DOM (Bercovici et al., 2023).

Surprisingly, we found no evidence for compartmentalised photodegradation between the SML and ULW. The simultaneous decline in AI_{mod}, humic-like FDOM, and I_{photo} across both layers indicated similar exposure to photodegradation rather than depth-specific processes. We attribute this to the SURF having only a shallow (1 m) water depth, allowing UV radiation to penetrate fully (Dring et al., 2001). In addition, the bright basin walls likely further enhanced UV exposure through reflection and scattering. Also, continuous slow pumping at the shallow SURF facility prevented stratification in the ULW (Bibi et al., 2025), limiting any segregation of photoreactive compounds into deeper water masses. It appears that the photosensitive molecular formulae contributing to I_{photo} were evenly distributed across the SURF, rather than selectively enriched in the SML, which prevented the detection of rapid, short-term (daily or sub-daily) photo effects. In comparison, Valderrama et al. (2025) observed enhanced photochemical activity of 17 low-molecular-weight, volatile compounds (< 92Da) in the SML during the same experiment. They furthermore suggested that OM photooxidation capacity is not influenced by phytoplankton bloom phases but mainly driven by redox-active species like iron. Combined, both results imply that SML- or ULW-specific photodegradation or photo-Fenton processes may affect compounds not captured by FT-ICR-MS or I_{photo}. It is however feasible, that I_{photo} in the SML, or other SML-specific compounds of the DOM geometabolome, are more affected than ULW in natural environments where light penetration into the water column is limited to depths < 1 m.

4.4 From mesocosm to ocean basin: Influence of phytoplankton-derived DOM on SML organic carbon dynamics

Scaling our observed SML enrichment to the mesocosm surface area (17 m^2) shows that a 1 mm SML with approximately 500 µM DOC would contain roughly 0.006 g C m^{-2}. Extrapolated to the global area of eutrophic coastal waters (~1.15×10^{12} m^2; Maúre et al., 2021), this corresponds to about 6.9×10^9 g C per week potentially retained in the SML during bloom conditions. That might be small relative to the global DOC inventory, yet locally significant given the SML's role as the interface for gas exchange and aerosol production. Since both *E. hux.* and *C. clos.* are cosmopolitan and major contributors to marine net

https://doi.org/10.5194/egusphere-2025-6563
Preprint. Discussion started: 13 January 2026

primary production (NPP), we suggest that their blooms, which substantially influence surface DOM composition, may disproportionally impact SML organic carbon budgets (Malviya et al., 2016). *E. hux.* forms extensive, recurrent blooms lasting several weeks across subpolar, temperate and coastal regions (2-10% of ocean NPP of 45-55 Pg C yr^{-1}: ~1-5 Pg C yr^{-1}; Poulton et al., 2007; Menschel et al., 2016; de Vries et al., 2024), and *C. clos.* is abundant in coastal and benthic habitats worldwide. Although species-specific shares of *C. clos.* are not known, diatoms are estimated to contribute ~20 % of NPP ~9-11 Pg C yr^{-1}; (Malviya et al., 2016). Assuming a combined coccolithophore and diatom production of 4-10 Pg C yr^{-1} DOC through exudation and cellular release, and considering that their abundance is expected to increase due to their competitive advantage in warming oceans (Chavez et al., 2011; Wurl et al., 2017; Wang et al., 2024), even modest enrichment at the microlayer scale has the potential to alter SML biogeochemistry on a global scale. Our mesocosm study was limited to a relatively small spatial and temporal scale, and due to the exclusion of wind-wave and rain- driven mixing, the life cycles of the detected biomolecules were artificially extended. While this setup allowed us to study the evolution of SML-DOM with unprecedented detail, future studies should focus on the biogeochemical succession of DOM quantity and composition over longer time periods to see which compounds may have longer residence times and thus a more persistent effect on air-sea interactions.

5 Conclusion

Our findings suggest that biogenically produced carbohydrates are the most likely and pronounced compound groups to accumulate in the DOM pool of the SML following phytoplankton blooms. The accumulation mechanism appears to be buoyancy-driven, as photosynthetically exuded polycarbonates aggregate into gel-like particles and float to the surface where they are subject to microbial and photochemical transformation. Our FT-ICR-MS and FTIR data further indicate accumulation of lipid- and protein-like DOM in the SML, while aromatic compounds and the bulk H/C ratio showed no compartmentalisation during and after the bloom. At the same time, photodegradation significantly altered DOM composition, but strong physical coupling in the mesocosm prevented surface-specific effects. We therefore propose that both buoyancy and polarity gradients are relevant, but polarity plays a minor role during and after the phytoplankton bloom. These results highlight the role of the polar fraction in SML-DOM composition in nutrient-rich marine environments. Enriched with labile DOM, the SML functions as a biogeochemical reactor and a hotspot for the turnover of diagenetically fixed carbon. The proportion of accumulated DOM in the SML could significantly influence air-gas exchange and the turnover time of carbon in coastal and upwelling environments during and after slick conditions, thereby affecting global carbon and trace gas fluxes. These processes underscore the sensitivity of the air-sea interface to changes in phytoplankton dynamics and emphasise the importance of explicitly incorporating carbohydrate-rich and surface-active assemblies in future models of air-sea exchange.

Competing interests

The authors declare that they have no conflict of interest.

Author contributions

https://doi.org/10.5194/egusphere-2025-6563
Preprint. Discussion started: 13 January 2026

JZ: Data Curation, Investigation, Formal Analysis, Methodology, Visualisation, Writing – Original Draft, Writing – Review & Editing, SS: Methodology, Investigation, Formal Analysis, Writing – review and editing, GF: Funding Acquisition, Formal Analysis, Supervision, Writing – Review & Editing, MR-R: Funding Acquisition, Conceptualisation, Supervision, Data Curation, Writing – Review & Editing, CL: Nutrients and Surfactants Sample Collection, Formal Analysis, Writing – Review & Editing, KP: Data Curation, Investigation, Methodology, Review & Editing, MP: Investigation, Writing – review and editing, HW: Data Curation, Funding Acquisition, Conceptualisation, Supervision, Project Administration, Writing – Review & Editing.

Financial support

This research was supported by the project "Biogeochemical processes and Air–sea exchange in the Sea-Surface microlayer (BASS)", which was funded by the German Research Foundation (DFG) under Grant No 451574234.

Acknowledgements

We thank Marit Renken for her valuable support during the laboratory work. We are also grateful to Ina Ulber, Matthias Friebe, Katrin Klaproth, and Heike Simon (ICBM, University of Oldenburg) for their indispensable assistance with DOC and DOM analyses. We acknowledge Prof. Dr. Oliver Wurl, spokesperson of the BASS project and head of the research group Processes and Sensorics of Marine Interfaces (ICBM, University of Oldenburg), for providing access to the experimental infrastructure SURF used in this study. We also thank all the BASS project scientists for their support in conducting this research. I acknowledge the use of AI in the generation of code structure and the refinement of text.

References

Abdulla, H.A.N., Minor, E.C., Dias, R.F., Hatcher, P.G., 2010. Changes in the compound classes of dissolved organic matter along an estuarine transect: A study using FTIR and 13C NMR. Geochimica et Cosmochimica Acta 74, 3815–3838. https://doi.org/10.1016/j.gca.2010.04.006

Allard, B., Borén, H., Pettersson, C., Zhang, G., 1994. Degradation of humic substances by UV irradiation. Environment International, The Fourth Nordic Symposium on Humic Substances 20, 97–101. https://doi.org/10.1016/0160-4120(94)90072-8

Artz, R.R.E., Chapman, S.J., Jean Robertson, A.H., Potts, J.M., Laggoun-Défarge, F., Gogo, S., Comont, L., Disnar, J.-R., Francez, A.-J., 2008. FTIR spectroscopy can be used as a screening tool for organic matter quality in regenerating cutover peatlands. Soil Biology and Biochemistry 40, 515–527. https://doi.org/10.1016/j.soilbio.2007.09.019

Asmussen-Schäfer, F., Ribas-Ribas, M., Wurl, O., Friedrichs, G., n.d. Linking surface coverage with surfactant activity – refining the role of surfactants for air-sea gas exchange. Biogeosciences/Ocean Sciences. https://cloud.rz.uni-kiel.de/index.php/s/dZSYntQAeyA4SB3

Badr, E.-S.A., Achterberg, E.P., Tappin, A.D., Hill, S.J., Braungardt, C.B., 2003. Determination of dissolved organic nitrogen in natural waters using high-temperature catalytic oxidation. TrAC Trends in Analytical Chemistry 22, 819–827. https://doi.org/10.1016/S0165-9936(03)01202-0

https://doi.org/10.5194/egusphere-2025-6563
Preprint. Discussion started: 13 January 2026

Balch, W.M., Holligan, P.M., Kilpatrick, K.A., 1992. Calcification, photosynthesis and growth of the bloom-forming coccolithophore, Emiliania huxleyi. Continental Shelf Research 12, 1353–1374. https://doi.org/10.1016/0278-4343(92)90059-S

Barthelmeß, T., Engel, A., 2022. How biogenic polymers control surfactant dynamics in the surface microlayer: insights from a coastal Baltic Sea study. Biogeosciences 19, 4965–4992. https://doi.org/10.5194/bg-19-4965-2022

Becker, S., Tebben, J., Coffinet, S., Wiltshire, K., Iversen, M.H., Harder, T., Hinrichs, K.-U., Hehemann, J.-H., 2020. Laminarin is a major molecule in the marine carbon cycle. Proc. Natl. Acad. Sci. U.S.A. 117, 6599–6607. https://doi.org/10.1073/pnas.1917001117

Bercovici, S.K., Wiemers, M., Dittmar, T., Niggemann, J., 2023. Disentangling Biological Transformations and Photodegradation Processes from Marine Dissolved Organic Matter Composition in the Global Ocean. Environ. Sci. Technol. 57, 21145–21155. https://doi.org/10.1021/acs.est.3c05929

Bergmann, D., Matarrita-Rodríguez, J., Abdulla, H., 2024. Toward a More Comprehensive Approach for Dissolved Organic Matter Chemical Characterization Using an Orbitrap Fusion Tribrid Mass Spectrometer Coupled with Ion and Liquid Chromatography Techniques. Anal. Chem. 96, 3744–3753. https://doi.org/10.1021/acs.analchem.3c02599

Bibi, R., Ribas-Ribas, M., Jaeger, L., Lehners, C., Gassen, L., Cortés, E., Wollschläger, J., Thölen, C., Waska, H., Zöbelein, J., Brinkhoff, T., Athale, I., Röttgers, R., Novak, M., Engel, A., Barthelmeß, T., Karnatz, J., Reinthaler, T., Spriahailo, D., Friedrichs, G., Schäfer, F., Wurl, O., 2025. Biogeochemical Dynamics of the Sea-Surface Microlayer in a Multidisciplinary Mesocosm Study. https://doi.org/10.5194/egusphere-2025-1773

Biersmith, A., Benner, R., 1998. Carbohydrates in phytoplankton and freshly produced dissolved organic matter. Marine Chemistry 63, 131–144. https://doi.org/10.1016/S0304-4203(98)00057-7

Böttcher, M.E., Oelschläger, B., Höpner, T., Brumsack, H.-J., Rullkötter, J., 1998. Sulfate reduction related to the early diagenetic degradation of organic matter and "black spot" formation in tidal sandflats of the German Wadden Sea (southern North Sea): stable isotope (13C, 34S, 18O) and other geochemical results. Organic Geochemistry 29, 1517–1530. https://doi.org/10.1016/S0146-6380(98)00124-7

Carlson, D.J., 1993. The Early Diagenesis of Organic Matter: Reaction at the Air-Sea Interface, in: Engel, M.H., Macko, S.A. (Eds.), Organic Geochemistry, Topics in Geobiology. Springer US, Boston, MA, pp. 255–268. https://doi.org/10.1007/978-1-4615-2890-6_12

Carlson, D.J., 1982. Surface microlayer phenolic enrichments indicate sea surface slicks. Nature 296, 426–429. https://doi.org/10.1038/296426a0

Carlson, D.J., Mayer, L.M., 1980. Enrichment of dissolved phenolic material in the surface microlayer of coastal waters. Nature 286, 482–483. https://doi.org/10.1038/286482a0

Celi, L., Schnitzer, M., Nègre, M., 1997. Analysis of Carboxyl Groups in Soil Humic Acids by a Wet Chemical Method, Fourier Transform Infrared Spectrophotometry, and Solution-State Carbon-13 Nuclear Magnetic Resonance: A Comparative Study. Soil Science 162, 189–197. https://doi.org/10.1097/00010694-199703000-00004

Chavez, F.P., Messié, M., Pennington, J.T., 2011. Marine Primary Production in Relation to Climate Variability and Change. Annual Review of Marine Science 3, 227–260. https://doi.org/10.1146/annurev.marine.010908.163917

Chin, W.-C., Orellana, M.V., Verdugo, P., 1998. Spontaneous assembly of marine dissolved organic matter into polymer gels. Nature 391, 568–572. https://doi.org/10.1038/35345

Coffey, N.R., Agblemanyo, F.E., McKenna, A.M., Wozniak, A.S., 2025a. Unsaturated aliphatic and sulfur-containing organic matter as surfactants in the surface microlayer. Marine Chemistry 272, 104547. https://doi.org/10.1016/j.marchem.2025.104547

Coffey, N.R., Agblemanyo, F.E., McKenna, A.M., Wozniak, A.S., 2025b. Unsaturated aliphatic and sulfur-containing organic matter as surfactants in the surface microlayer. Marine Chemistry 272, 104547. https://doi.org/10.1016/j.marchem.2025.104547

Corzo, A., Morillo, J.A., Rodríguez, S., 2000. Production of transparent exopolymer particles (TEP) in cultures of Chaetoceros calcitrans under nitrogen limitation. Aquatic Microbial Ecology 23, 63–72. https://doi.org/10.3354/ame023063

Croot, P.L., Passow, U., Assmy, P., Jansen, S., Strass, V.H., 2007. Surface active substances in the upper water column during a Southern Ocean Iron Fertilization Experiment (EIFEX). Geophysical Research Letters 34. https://doi.org/10.1029/2006GL028080

https://doi.org/10.5194/egusphere-2025-6563
Preprint. Discussion started: 13 January 2026

Cunliffe, M., Engel, A., Frka, S., Gašparović, B., Guitart, C., Murrell, J.C., Salter, M., Stolle, C., Upstill-Goddard, R., Wurl, O., 2013. Sea surface microlayers: A unified physicochemical and biological perspective of the air–ocean interface. Progress in Oceanography 109, 104–116. https://doi.org/10.1016/j.pocean.2012.08.004

Cunliffe, M., Murrell, J.C., 2009. The sea-surface microlayer is a gelatinous biofilm. The ISME Journal 2009 3:9 3, 1001–1003. https://doi.org/10.1038/ismej.2009.69

Cunliffe, M., Wurl, O., 2014. Guide to best practices to study the ocean's surface. Occasional Publications of the Marine Biological Association of the United Kingdom, Plymouth, UK.

D'Andrilli, J., Cooper, W.T., Foreman, C.M., Marshall, A.G., 2015. An ultrahigh-resolution mass spectrometry index to estimate natural organic matter lability. Rapid Communications in Mass Spectrometry 29, 2385–2401. https://doi.org/10.1002/rcm.7400

D'Andrilli, J., Junker, J.R., Smith, H.J., Scholl, E.A., Foreman, C.M., 2019. DOM composition alters ecosystem function during microbial processing of isolated sources. Biogeochemistry 142, 281–298. https://doi.org/10.1007/s10533-018-00534-5

de Vries, J., Poulton, A.J., Young, J.R., Monteiro, F.M., Sheward, R.M., Johnson, R., Hagino, K., Ziveri, P., Wolf, L.J., 2024. CASCADE: Dataset of extant coccolithophore size, carbon content and global distribution. Sci Data 11, 920. https://doi.org/10.1038/s41597-024-03724-z

Dittmar, T., Koch, B., Hertkorn, N., Kattner, G., 2008. A simple and efficient method for the solid-phase extraction of dissolved organic matter (SPE-DOM) from seawater. Limnology and Oceanography: Methods 6, 230–235. https://doi.org/10.4319/lom.2008.6.230

Dring, M.J., Wagner, A., Franklin, L.A., Kuhlenkamp, R., Lüning, K., 2001. Seasonal and diurnal variations in ultraviolet-B and ultraviolet-A irradiances at and below the sea surface at Helgoland (North Sea) over a 6-year period. Helgol Mar Res 55, 3–11. https://doi.org/10.1007/s101520000063

Duan, J., Sontarp, E.J., Myneni, S.C.B., 2024. Detecting Structural Environments of Carboxyl Groups in Dissolved Natural Organic Molecules. ACS EST Water 4, 555–563. https://doi.org/10.1021/acsestwater.3c00609

Elliott, S., Burrows, S., Cameron-Smith, P., Hoffman, F., Hunke, E., Jeffery, N., Liu, Y., Maltrud, M., Menzo, Z., Ogunro, O., Van Roekel, L., Wang, S., Brunke, M., Jin, M., Letscher, R., Meskhidze, N., Russell, L., Simpson, I., Stokes, D., Wingenter, O., 2018. Does Marine Surface Tension Have Global Biogeography? Addition for the OCEANFILMS Package. Atmosphere 9, 216. https://doi.org/10.3390/atmos9060216

Ellison, G.B., Tuck, A.F., Vaida, V., 1999. Atmospheric processing of organic aerosols. Journal of Geophysical Research: Atmospheres 104, 11633–11641. https://doi.org/10.1029/1999JD900073

Engel, A., Bange, H.W., Cunliffe, M., Burrows, S.M., Friedrichs, G., Galgani, L., Herrmann, H., Hertkorn, N., Johnson, M., Liss, P.S., Quinn, P.K., Schartau, M., Soloviev, A., Stolle, C., Upstill-Goddard, R.C., van Pinxteren, M., Zäncker, B., 2017. The Ocean's Vital Skin: Toward an Integrated Understanding of the Sea Surface Microlayer. Front. Mar. Sci. 4. https://doi.org/10.3389/fmars.2017.00165

Engel, A., Delille, B., Jacquet, S., Riebesell, U., Rochelle-Newall, E., Terbrüggen, A., Zondervan, I., 2004. Transparent exopolymer particles and dissolved organic carbon production by Emiliania huxleyi exposed to different CO2 concentrations: a mesocosm experiment. Aquatic Microbial Ecology 34, 93–104. https://doi.org/10.3354/ame034093

Engel, A., Passow, U., 2001. Carbon and nitrogen content of transparent exopolymer particles (TEP) in relation to their Alcian Blue adsorption. Marine Ecology Progress Series 219, 1–10. https://doi.org/10.3354/meps219001

Field, C.B., Behrenfeld, M.J., Randerson, J.T., Falkowski, P., 1998. Primary Production of the Biosphere: Integrating Terrestrial and Oceanic Components. Science 281, 237–240. https://doi.org/10.1126/science.281.5374.237

Flerus, R., Lechtenfeld, O.J., Koch, B.P., McCallister, S.L., Schmitt-Kopplin, P., Benner, R., Kaiser, K., Kattner, G., 2012. A molecular perspective on the ageing of marine dissolved organic matter. Biogeosciences 9, 1935–1955. https://doi.org/10.5194/bg-9-1935-2012

Frew, N.M., Nelson, R.K., Johnson, C.G., 2006. Sea slicks: variability in chemical composition and surface elasticity, in: Gade, M., Hühnerfuss, H., Korenowski, G.M. (Eds.), Marine Surface Films: Chemical Characteristics, Influence on Air-Sea Interactions and Remote Sensing. Springer, Berlin, Heidelberg, pp. 45–56. https://doi.org/10.1007/3-540-33271-5_6

https://doi.org/10.5194/egusphere-2025-6563
Preprint. Discussion started: 13 January 2026

Gašparović, B., Ćosović, B., Vojvodić, V., 1998. Contribution of organic acids to the pool of surface active substances in model and marine samples using *o*-nitrophenol as an electrochemical probe. Organic Geochemistry 29, 1025–1032. https://doi.org/10.1016/S0146-6380(98)00055-2

Gašparović, Blaženka, Kozarac, Z., Saliot, A., Ćosović, B., Möbius, D., 1998a. Physicochemical Characterization of Natural and*ex-Situ*Reconstructed Sea-Surface Microlayers. Journal of Colloid and Interface Science 208, 191–202. https://doi.org/10.1006/jcis.1998.5792

Gašparović, Blaženka, Vojvodić, V., Ćosović, B., 1998b. Excretion of Organic Matter during an Experimental Phytoplankton Bloom Followed Using *o*-Nitrophenol as an Electrochemical Probe. Croatica Chemica Acta 71, 271–284.

Gautam, K. k., Tyagi, V. k., 2006. Microbial Surfactants: A Review. Journal of Oleo Science 55, 155–166. https://doi.org/10.5650/jos.55.155

Goes, J.I., Handa, N., Taguchi, S., Hama, T., Saito, H., 1996. Metabolism of neutral monosaccharide constituents of storage and structural carbohydrates in natural assemblages of marine phytoplankton exposed to ultraviolet radiation. Limnology and Oceanography 41, 1478–1489. https://doi.org/10.4319/lo.1996.41.7.1478

Gonsior, M., Peake, B.M., Cooper, W.T., Podgorski, D., D'Andrilli, J., Cooper, W.J., 2009. Photochemically Induced Changes in Dissolved Organic Matter Identified by Ultrahigh Resolution Fourier Transform Ion Cyclotron Resonance Mass Spectrometry. Environ. Sci. Technol. 43, 698–703. https://doi.org/10.1021/es8022804

Griffiths, P.R., Haseth, J.A., 2007. Fourier Transform Infrared Spectrometry, 2nd ed. Wiley: Hoboken.

Grossart, H., Engel, A., Arnosti, C., De La Rocha, C., Murray, A., Passow, U., 2007. Microbial dynamics in autotrophic and heterotrophic seawater mesocosms. III. Organic matter fluxes. Aquat. Microb. Ecol. 49, 143–156. https://doi.org/10.3354/ame01140

Hammer, K., Kattner, G., 1986. Dissolved free amino acids in the marine environment: a carbon to nitrogen ratio shift during diatom blooms. Mar. Ecol. Prog. Ser. 31, 35–45. https://doi.org/10.3354/meps031035

He, W., Chen, M., Schlautman, M.A., Hur, J., 2016. Dynamic exchanges between DOM and POM pools in coastal and inland aquatic ecosystems: A review. Science of The Total Environment 551–552, 415–428. https://doi.org/10.1016/j.scitotenv.2016.02.031

Hunter, K.A., Liss, P.S., 1981. Chapter 9 Organic Sea Surface Films, in: Duursma, E.K., Dawson, R. (Eds.), Elsevier Oceanography Series, Marine Organic Chemistry. Elsevier, pp. 259–298. https://doi.org/10.1016/S0422-9894(08)70331-3

Ittekkot, V., Brockmann, U., Michaelis, W., Degens, E.T., 1981. Dissolved Free and Combined Carbohydrates During a Phytoplankton Bloom in the Northern North Sea. Marine Ecology Progress Series 4, 299–305.

Jibaja Valderrama, O., Scheres Firak, D., Schaefer, T., van Pinxteren, M., Fomba, K.W., Herrmann, H., 2025. Photochemistry of the sea-surface microlayer (SML) influenced by a phytoplankton bloom: A mesocosm study. EGUsphere 1–32. https://doi.org/10.5194/egusphere-2025-4066

Kepkay, P., Jellett, J., Niven, S., 1997. Respiration and the carbon-to-nitrogen ratio of a phytoplankton bloom. Mar. Ecol. Prog. Ser. 150, 249–261. https://doi.org/10.3354/meps150249

Kim, Dong Hyun, Kim, Do Hyoung, Lee, S.-H., Kim, K.H., 2018. A novel β-glucosidase from Saccharophagus degradans 2-40T for the efficient hydrolysis of laminarin from brown macroalgae. Biotechnology for Biofuels 11, 64. https://doi.org/10.1186/s13068-018-1059-2

Kitaoka, M., Matsuoka, Y., Mori, K., Nishimoto, M., Hayashi, K., 2012. Characterization of a Bacterial Laminaribiose Phosphorylase. Bioscience, Biotechnology, and Biochemistry 76, 343–348. https://doi.org/10.1271/bbb.110772

Koch, B.P., Dittmar, T., 2006. From mass to structure: an aromaticity index for high-resolution mass data of natural organic matter. Rapid Communications in Mass Spectrometry 20, 926–932. https://doi.org/10.1002/rcm.2386

Koch, B.P., Kattner, G., Witt, M., Passow, U., 2014. Molecular insights into the microbial formation of marine dissolved organic matter: recalcitrant or labile? Biogeosciences 11, 4173–4190. https://doi.org/10.5194/bg-11-4173-2014

Koch, B.P., Ludwichowski, K.-U., Kattner, G., Dittmar, T., Witt, M., 2008. Advanced characterization of marine dissolved organic matter by combining reversed-phase liquid chromatography and FT-ICR-MS. Marine Chemistry 111, 233–241. https://doi.org/10.1016/j.marchem.2008.05.008

Kumagai, Y., Satoh, T., Inoue, A., Ojima, T., 2014. A laminaribiose-hydrolyzing enzyme, AkLab, from the common sea hare Aplysia kurodai and its transglycosylation activity. Comparative Biochemistry and Physiology Part B: Biochemistry and Molecular Biology 167, 1–7. https://doi.org/10.1016/j.cbpb.2013.07.008

https://doi.org/10.5194/egusphere-2025-6563
Preprint. Discussion started: 13 January 2026

Kumar, M., Tibocha-Bonilla, J.D., Füssy, Z., Lieng, C., Schwenck, S.M., Levesque, A.V., Al-Bassam, M.M., Passi, A., Neal, M., Zuniga, C., Kaiyom, F., Espinoza, J.L., Lim, H., Polson, S.W., Allen, L.Z., Zengler, K., 2024. Mixotrophic growth of a ubiquitous marine diatom. Science Advances 10, eado2623. https://doi.org/10.1126/sciadv.ado2623

Laß, K., Friedrichs, G., 2011. Revealing structural properties of the marine nanolayer from vibrational sum frequency generation spectra. Journal of Geophysical Research: Oceans 116. https://doi.org/10.1029/2010JC006609

Laß, K., Bange, H.W., Friedrichs, G., 2013. Seasonal signatures in SFG vibrational spectra of the sea surface nanolayer at Boknis Eck Time Series Station (SW Baltic Sea). Biogeosciences 10, 5325–5334. https://doi.org/10.5194/bg-10-5325-2013

Lavaud, J., Rousseau, B., Etienne, A., 2004. GENERAL FEATURES OF PHOTOPROTECTION BY ENERGY DISSIPATION IN PLANKTONIC DIATOMS (BACILLARIOPHYCEAE)[1]. Journal of Phycology 40, 130–137. https://doi.org/10.1046/j.1529-8817.2004.03026.x

Lechtenfeld, O.J., Koch, B.P., Gašparović, B., Frka, S., Witt, M., Kattner, G., 2013. The influence of salinity on the molecular and optical properties of surface microlayers in a karstic estuary. Marine Chemistry 150, 25–38. https://doi.org/10.1016/j.marchem.2013.01.006

Liss, P.S., Duce, R.A., 1997. The Sea Surface and Global Change, The Sea Surface and Global Change.

Liu, Z., Sleighter, R.L., Zhong, J., Hatcher, P.G., 2011. The chemical changes of DOM from black waters to coastal marine waters by HPLC combined with ultrahigh resolution mass spectrometry. Estuarine, Coastal and Shelf Science 92, 205–216. https://doi.org/10.1016/j.ecss.2010.12.030

Logan, B.E., Passow, U., Alldredge, A.L., Grossartt, H.-P., Simont, M., 1995. Rapid formation and sedimentation of large aggregates is predictable from coagulation rates (half-lives) of transparent exopolymer particles (TEP). Deep Sea Research Part II: Topical Studies in Oceanography 42, 203–214. https://doi.org/10.1016/0967-0645(95)00012-F

Malviya, S., Scalco, E., Audic, S., Vincent, F., Veluchamy, A., Poulain, J., Wincker, P., Iudicone, D., de Vargas, C., Bittner, L., Zingone, A., Bowler, C., 2016. Insights into global diatom distribution and diversity in the world's ocean. Proceedings of the National Academy of Sciences 113, E1516–E1525. https://doi.org/10.1073/pnas.1509523113

Marty, J.C., Saliot, A., 1976. Hydrocarbons (normal alkanes) in the surface microlayer of seawater. Deep Sea Research and Oceanographic Abstracts 23, 863–873. https://doi.org/10.1016/0011-7471(76)90853-6

Marty, J.C., Saliot, A., Buat-Ménard, P., Chesselet, R., Hunter, K.A., 1979. Relationship between the lipid compositions of marine aerosols, the sea surface microlayer, and subsurface water. Journal of Geophysical Research: Oceans 84, 5707–5716. https://doi.org/10.1029/JC084iC09p05707

Maúre, E.D.R., Terauchi, G., Ishizaka, J., Clinton, N., DeWitt, M., 2021. Globally consistent assessment of coastal eutrophication. Nat Commun 12, 6142. https://doi.org/10.1038/s41467-021-26391-9

Menschel, E., González, H.E., Giesecke, R., 2016. Coastal-oceanic distribution gradient of coccolithophores and their role in the carbonate flux of the upwelling system off Concepción, Chile (36°S). J. Plankton Res. 38, 798–817. https://doi.org/10.1093/plankt/fbw037

Merder, J., Freund, J.A., Feudel, U., Hansen, C.T., Hawkes, J.A., Jacob, B., Klaproth, K., Niggemann, J., Noriega-Ortega, B.E., Osterholz, H., Rossel, P.E., Seidel, M., Singer, G., Stubbins, A., Waska, H., Dittmar, T., 2020. ICBM-OCEAN: Processing Ultrahigh-Resolution Mass Spectrometry Data of Complex Molecular Mixtures. Anal. Chem. 92, 6832–6838. https://doi.org/10.1021/acs.analchem.9b05659

Miller, W.L., Moran, M.A., 1997. Interaction of photochemical and microbial processes in the degradation of refractory dissolved organic matter from a coastal marine environment. Limnology & Oceanography 42, 1317–1324. https://doi.org/10.4319/lo.1997.42.6.1317

Minor, E., Stephens, B., 2008. Dissolved organic matter characteristics within the Lake Superior watershed. Organic Geochemistry 39, 1489–1501. https://doi.org/10.1016/j.orggeochem.2008.08.001

Minor, E.C., Swenson, M.M., Mattson, B.M., Oyler, A.R., 2014. Structural characterization of dissolved organic matter: a review of current techniques for isolation and analysis. Environ. Sci.: Processes Impacts 16, 2064–2079. https://doi.org/10.1039/C4EM00062E

Mopper, K., zhou, J., Sri Ramana, K., passow, U., dam, H.G., Drapeau, D.T., 1995. The role of surface-active carbohydrates in the flocculation of a diatom bloom in a mesocosm. Deep Sea Research Part II: Topical Studies in Oceanography 42, 47–73. https://doi.org/10.1016/0967-0645(95)00004-A

https://doi.org/10.5194/egusphere-2025-6563
Preprint. Discussion started: 13 January 2026

Moran, M.A., Ferrer-González, F.X., Fu, H., Nowinski, B., Olofsson, M., Powers, M.A., Schreier, J.E., Schroer, W.F., Smith, C.B., Uchimiya, M., 2022. The Ocean's labile DOC supply chain. Limnology and Oceanography 67, 1007–1021. https://doi.org/10.1002/lno.12053

Moran, M.A., Sheldon, W.M., Zepp, R.G., 2000. Carbon loss and optical property changes during long-term photochemical and biological degradation of estuarine dissolved organic matter. Limnology & Oceanography 45, 1254–1264. https://doi.org/10.4319/lo.2000.45.6.1254

Moran, M.A., Zepp, R.G., 1997. Role of photoreactions in the formation of biologically labile compounds from dissolved organic matter. Limnology and Oceanography 42, 1307–1316. https://doi.org/10.4319/lo.1997.42.6.1307

Myklestad, S.M., 1995. Release of extracellular products by phytoplankton with special emphasis on polysaccharides. Science of The Total Environment, Marine Mucilages 165, 155–164. https://doi.org/10.1016/0048-9697(95)04549-G

Niggemann, J., Gerdts, G., Dittmar, T., 2011. Geo-metabolomics A key for understanding function and reactivity of dissolved organic matter, in: EPIC3Goldschmidt Conference 2011, Prague. Presented at the Goldschmidt Conference 2011, Prague.Ortega-Retuerta, E., Passow, U., Duarte, C.M., Reche, I., 2009. Effects of ultraviolet B radiation on (not so) transparent exopolymer particles. Biogeosciences 6, 3071–3080. https://doi.org/10.5194/bg-6-3071-2009

Pärnpuu, S., Astover, A., Tõnutare, T., Penu, P., Kauer, K., 2022. Soil organic matter qualification with FTIR spectroscopy under different soil types in Estonia. Geoderma Regional 28, e00483. https://doi.org/10.1016/j.geodrs.2022.e00483

Passow, U., 2002. Transparent exopolymer particles (TEP) in aquatic environments. Progress in Oceanography 55, 287–333. https://doi.org/10.1016/S0079-6611(02)00138-6

Passow, U., 2000. Formation of transparent exopolymer particles, TEP, from dissolved precursor material. Marine Ecology Progress Series 192, 1–11. https://doi.org/10.3354/meps192001

Passow, U., Alldredge, A.L., Logan, B.E., 1994. The role of particulate carbohydrate exudates in the flocculation of diatom blooms. Deep Sea Research Part I: Oceanographic Research Papers 41, 335–357. https://doi.org/10.1016/0967-0637(94)90007-8

Passow, U., Engel, A., 2001. The Role of Transparent Exopolymer Particles (TEP) in determining C:N ratios of particulate matter. Presented at the ASLO Aquatic Sciences Meeting 2001, Albuquerque, USA.

Penna, A., 1999. Influence of nutrient ratios on the in vitro extracellular polysaccharide production by marine diatoms from the Adriatic Sea. Journal of Plankton Research 21, 1681–1690. https://doi.org/10.1093/plankt/21.9.1681

Petras, D., Koester, I., Da Silva, R., Stephens, B.M., Haas, A.F., Nelson, C.E., Kelly, L.W., Aluwihare, L.I., Dorrestein, P.C., 2017. High-Resolution Liquid Chromatography Tandem Mass Spectrometry Enables Large Scale Molecular Characterization of Dissolved Organic Matter. Front. Mar. Sci. 4. https://doi.org/10.3389/fmars.2017.00405

Poulton, A.J., Adey, T.R., Balch, W.M., Holligan, P.M., 2007. Relating coccolithophore calcification rates to phytoplankton community dynamics: Regional differences and implications for carbon export. Deep Sea Research Part II: Topical Studies in Oceanography 54, 538–557. https://doi.org/10.1016/j.dsr2.2006.12.003

Raeke, J., Lechtenfeld, O.J., Wagner, M., Herzsprung, P., Reemtsma, T., 2016. Selectivity of solid phase extraction of freshwater dissolved organic matter and its effect on ultrahigh resolution mass spectra. Environ. Sci.: Processes Impacts 18, 918–927. https://doi.org/10.1039/C6EM00200E

R Core Team (2025). *R: A language and environment for statistical computing*. R Foundation for Statistical Computing, Vienna, Austria. URL https://www.R-project.org/

Rickard, P.C., Uher, G., Upstill-Goddard, R.C., Frka, S., Mustaffa, N.I.H., Banko-Kubis, H.M., Cvitešić Kušan, A., Gašparović, B., Stolle, C., Wurl, O., Ribas-Ribas, M., 2019. Reconsideration of seawater surfactant activity analysis based on an inter-laboratory comparison study. Marine Chemistry 208, 103–111. https://doi.org/10.1016/j.marchem.2018.11.012

Sadat, A., Joye, I.J., 2020. Peak Fitting Applied to Fourier Transform Infrared and Raman Spectroscopic Analysis of Proteins. Applied Sciences 10, 5918. https://doi.org/10.3390/app10175918

Sakugawa, H., Handa, N., Ohta, K., 1985. Isolation and characterization of low molecular weight carbohydrates dissolved in seawater. Marine Chemistry 17, 341–362. https://doi.org/10.1016/0304-4203(85)90007-6

Schmitt-Kopplin, P., Liger-Belair, G., Koch, B.P., Flerus, R., Kattner, G., Harir, M., Kanawati, B., Lucio, M., Tziotis, D., Hertkorn, N., Gebefügi, I., 2012. Dissolved organic matter in sea spray: a transfer study from marine surface water to aerosols. Biogeosciences 9, 1571–1582. https://doi.org/10.5194/bg-9-1571-2012

https://doi.org/10.5194/egusphere-2025-6563
Preprint. Discussion started: 13 January 2026

Schnetger, B., Lehners, C., 2014. Determination of nitrate plus nitrite in small volume marine water samples using vanadium(III)chloride as a reduction agent. Marine Chemistry 160, 91–98. https://doi.org/10.1016/j.marchem.2014.01.010

Scholz, B., Rúa, A., Liebezeit, G., 2014. Effects of UV radiation on five marine microphytobenthic Wadden sea diatoms, isolated from the Solthörn tidal flat (Lower Saxony, southern North Sea) – Part II: changes in carbohydrate, amino acid and fatty acid composition. European Journal of Phycology 49, 97–114. https://doi.org/10.1080/09670262.2014.893589

Seidel, M., Beck, M., Greskowiak, J., Riedel, T., Waska, H., Suryaputra, Ig.N.A., Schnetger, B., Niggemann, J., Simon, M., Dittmar, T., 2015. Benthic-pelagic coupling of nutrients and dissolved organic matter composition in an intertidal sandy beach. Marine Chemistry 176, 150–163. https://doi.org/10.1016/j.marchem.2015.08.011

Seidel, M., Beck, M., Riedel, T., Waska, H., Suryaputra, I.G.N.A., Schnetger, B., Niggemann, J., Simon, M., Dittmar, T., 2014. Biogeochemistry of dissolved organic matter in an anoxic intertidal creek bank. Geochimica et Cosmochimica Acta 140, 418–434. https://doi.org/10.1016/j.gca.2014.05.038

Setschenow, J., 1889. Über die Konstitution der Salzlösungen auf Grund ihres Verhaltens zu Kohlensäure. Zeitschrift für Physikalische Chemie 4U, 117–125. https://doi.org/10.1515/zpch-1889-0409

Silva, A.N., Nikzad, S., Barthelmeß, T., Engel, A., Hermann, H., Van Pinxteren, M., Wirtz, K., Wurl, O., Schartau, M., 2025. Meta-analytical insights into organic matter enrichment in the surface microlayer. https://doi.org/10.5194/egusphere-2025-4050

Socrates, G., 2004. Infrared and Raman Characteristic Group Frequencies: Tables and Charts. John Wiley & Sons.

Soong, J.L., Calderón, F.J., Betzen, J., Cotrufo, M.F., 2014. Quantification and FTIR characterization of dissolved organic carbon and total dissolved nitrogen leached from litter: a comparison of methods across litter types. Plant Soil 385, 125–137. https://doi.org/10.1007/s11104-014-2232-4

Stubbins, A., Dittmar, T., 2015. Illuminating the deep: Molecular signatures of photochemical alteration of dissolved organic matter from North Atlantic Deep Water. Marine Chemistry, Biogeochemistry of dissolved organic matter 177, 318–324. https://doi.org/10.1016/j.marchem.2015.06.020

Stubbins, A., Spencer, R.G.M., Chen, H., Hatcher, P.G., Mopper, K., Hernes, P.J., Mwamba, V.L., Mangangu, A.M., Wabakanghanzi, J.N., Six, J., 2010. Illuminated darkness: Molecular signatures of Congo River dissolved organic matter and its photochemical alteration as revealed by ultrahigh precision mass spectrometry. Limnology and Oceanography 55, 1467–1477. https://doi.org/10.4319/lo.2010.55.4.1467

Sugimura, Y., Suzuki, Y., 1988. A high-temperature catalytic oxidation method for the determination of non-volatile dissolved organic carbon in seawater by direct injection of a liquid sample. Marine Chemistry 24, 105–131. https://doi.org/10.1016/0304-4203(88)90043-6

Thornton, D.C.O., 2014. Dissolved organic matter (DOM) release by phytoplankton in the contemporary and future ocean. European Journal of Phycology 49, 20–46. https://doi.org/10.1080/09670262.2013.875596

Underwood, G.J.C., Nilsson, C., Sundbäck, K., Wulff, A., 1999. Short-Term Effects of Uvb Radiation on Chlorophyll Fluorescence, Biomass, Pigments, and Carbohydrate Fractions in a Benthic Diatom Mat. Journal of Phycology 35, 656–666. https://doi.org/10.1046/j.1529-8817.1999.3540656.x

Van Den Meersche, K., Middelburg, J.J., Soetaert, K., Van Rijswijk, P., Boschker, H.T.S., Heip, C.H.R., 2004. Carbon-nitrogen coupling and algal-bacterial interactions during an experimental bloom: Modeling a ^{13}C tracer experiment. Limnology & Oceanography 49, 862–878. https://doi.org/10.4319/lo.2004.49.3.0862

Van Oostende, N., Moerdijk-Poortvliet, T.C.W., Boschker, H.T.S., Vyverman, W., Sabbe, K., 2013. Release of dissolved carbohydrates by Emiliania huxleyi and formation of transparent exopolymer particles depend on algal life cycle and bacterial activity. Environ Microbiol 15, 1514–1531. https://doi.org/10.1111/j.1462-2920.2012.02873.x

Wang, J., Zeng, C., Feng, Y., 2024. Meta-analysis reveals responses of coccolithophores and diatoms to warming. Marine Environmental Research 193, 106275. https://doi.org/10.1016/j.marenvres.2023.106275

Waska, H., Banko-Kubis, H.M., 2024. Dissolved organic matter released from beach wrack is source-specific and molecularly highly diverse. Biogeochemistry 167, 1057–1078. https://doi.org/10.1007/s10533-024-01159-7

Waska, H., Simon, H., Ahmerkamp, S., Greskowiak, J., Ahrens, J., Seibert, S.L., Schwalfenberg, K., Zielinski, O., Dittmar, T., 2021. Molecular Traits of Dissolved Organic Matter in the Subterranean Estuary of a High-Energy Beach: Indications of Sources and Sinks. Front. Mar. Sci. 8, 607083. https://doi.org/10.3389/fmars.2021.607083

https://doi.org/10.5194/egusphere-2025-6563
Preprint. Discussion started: 13 January 2026

Weeks, A.R., Fasham, M.J.R., Aiken, J., Harbour, D.S., Read, J.F., Bellan, I., 1993. The spatial and temporal development of the spring bloom during the JGOFS North Atlantic Bloom Experiment, 1989. Journal of the Marine Biological Association of the United Kingdom 73, 253–282. https://doi.org/10.1017/S0025315400032847

Wood, A.M., Van Valen, L.M., 1990. Paradox lost on the release of energy rich compounds by phytoplankton. Marine Microbial Food Webs 4, 103–116.

Wurl, O., Ekau, W., Landing, W.M., Zappa, C.J., 2017. Sea surface microlayer in a changing ocean - A perspective. Elementa 5, 31. https://doi.org/10.1525/ELEMENTA.228/112437

Wurl, O., Holmes, M., 2008. The gelatinous nature of the sea-surface microlayer. Marine Chemistry 110, 89–97. https://doi.org/10.1016/j.marchem.2008.02.009

Wurl, O., Miller, L., Röttgers, R., Vagle, S., 2009. The distribution and fate of surface-active substances in the sea-surface microlayer and water column. Marine Chemistry 115, 1–9. https://doi.org/10.1016/J.MARCHEM.2009.04.007

Wurl, O., Miller, L., Vagle, S., 2011. Production and fate of transparent exopolymer particles in the ocean. J. Geophys. Res. 116. https://doi.org/10.1029/2011jc007342

Wurl, O., Obbard, J.P., 2004. A review of pollutants in the sea-surface microlayer (SML): a unique habitat for marine organisms. Marine Pollution Bulletin 48, 1016–1030. https://doi.org/10.1016/j.marpolbul.2004.03.016

Xie, W.-H., Shiu, W.-Y., Mackay, D., 1997. A review of the effect of salts on the solubility of organic compounds in seawater. Marine Environmental Research 44, 429–444. https://doi.org/10.1016/S0141-1136(97)00017-2

Zark, M., Christoffers, J., Dittmar, T., 2017. Molecular properties of deep-sea dissolved organic matter are predictable by the central limit theorem: Evidence from tandem FT-ICR-MS. Marine Chemistry 191, 9–15. https://doi.org/10.1016/j.marchem.2017.02.005

Zhou, J., Mopper, K., Passow, U., 1998. The role of surface-active carbohydrates in the formation of transparent exopolymer particles by bubble adsorption of seawater. Limnology and Oceanography 43, 1860–1871. https://doi.org/10.4319/lo.1998.43.8.1860

Žutić, V., Ćosović, B., Marčenko, E., Bihari, N., Kršinić, F., 1981. Surfactant production by marine phytoplankton. Marine Chemistry 10, 505–520. https://doi.org/10.1016/0304-4203(81)90004-9